Composition of rare earth elements in settling particles collected in the highly productive North Pacific Ocean and Bering Sea : Implications for siliceous-matter dissolution kinetics and formation of two REE-enriched phases

Akagi, Tasuku
Department of Earth and Planetary Sciences, Faculty of Sciences, Kyushu University

Fu, Feng-fu
Key Lab of Analysis and Detecting Technology for Food Safety (Fuzhou University) of Ministry of Education, Fuzhou University

Hongo, Yayoi
The Institute of Physical and Chemical Research (RIKEN), Molecular Characterization Team

Takahashi, Kozo
Department of Earth and Planetary Sciences, Faculty of Sciences, Kyushu University

出版情報：Geochimica et Cosmochimica Acta. 75 (17), pp.4857-4876, 2011-09-01. Elsevier
バージョン：

Composition of Rare Earth Elements in Settling Particles Collected in the Highly Productive North Pacific Ocean and Bering Sea: Implications for Siliceous-Matter Dissolution Kinetics and Formation of Two REE-Enriched Phases

Tasuku AKAGI[1], Feng-fu FU[2], Yayoi HONGO[3], and Kozo TAKAHASHI[1]

[1]Department of Earth and Planetary Sciences, Faculty of Sciences, 33 Kyushu University, 6-10-1 Hakozaki, Higashi-ku, Fukuoka 812-8581, Japan
[2]Key Lab of Analysis and Detecting Technology for Food Safety (Fuzhou University) of Ministry of Education, Fuzhou University, Fuzhou, Fujian 350002, China
[3]The Institute of Physical and Chemical Research (RIKEN), Molecular Characterization Team, 2-1, Hirosawa, Wako, Saitama 351-0198, Japan

Abstract

Settling particles were sampled monthly for one year using an automated time-series sediment trap positioned at similar depths at two sites of high diatomaceous productivity in the North Pacific Ocean and Bering Sea. The particles were analyzed for rare earth elements (REEs) by inductively coupled plasma mass spectrometry (ICP–MS) with and without chemical treatment of the bulk samples to isolate siliceous fractions. The REE composition of the bulk samples is explained largely by the contribution of two distinct components: i) carbonate with a higher REE concentration, a negative Ce anomaly and lighter REE (LREE) enrichment; ii) opal with a lower REE concentration, a weaker negative Ce anomaly and heavier REE (HREE) enrichment.

The siliceous fractions of settling particles are characterized by high Si/Al ratios (30-70), reflecting high diatom productivity at the studied sites. The La/Al ratio of the siliceous fraction is close to that of the upper crust, but the Lu/Al and Lu/La ratios are significantly higher than those of the upper crust or airborne particles, indicating the presence of excess HREEs in the siliceous fraction. Diatoms are believed to be important carriers of HREEs.

The Ce anomaly, Eu anomaly, slope of the REE pattern, and ΣREE of the siliceous fraction vary exponentially with decreasing total mass flux. They can be

well-reproduced according to the differential dissolution kinetics of elements in the order of Ce < lighter REEs (LREEs) < Eu = heavier REEs (HREEs) < Si from settling particles, where the dissolution rate is critically reduced through particle aggregation. This order is consistent with the vertical distribution of dissolved REEs and Si in oceans. The differential dissolution kinetics leads to HREE enrichment of the original diatoms. The Lu/Si ratio of the siliceous fraction of settling particles recovered from some of the highest diatom fluxes is identical to that of the two elements dissolved in deep seawater, providing further evidence for the dissolution of siliceous matter in deep water.

Introduction

As marine particles settle through a seawater column, they are in contact with and exchange elements with the dissolved phase. Settling particles play an important role in material transport through the water column and an understanding of their dynamic behavior is critical to determine the proportion of elements that are removed from or recycled into the column.

Many studies have addressed issues related to settling particles, including particle formation, particle size change, aggregation rate, regeneration, disintegration rate, settling speed, compositional variation, and productivity in surface water. These studies are well summarized in reviews by Anderson (2006) and Archer (2006). Nevertheless, the geochemical behavior of settling particles is complicated and a clear understanding of their dynamics has not been adequately achieved (e.g., Archer, 2006).

Rare earth elements (REEs) are a unique set of elements. They behave in a coherent manner with respect to one another because of the unique electronic configuration of their ions: the number of inner 4f shells increases systematically with increasing atomic number, leaving the outermost shell identical among these elements. Two elements distinguish themselves among this group and offer the possibility of using the group as a geochemical tracer. Cerium can adopt a valency of 4+ or 3+ in aqueous environments and, accordingly, behaves differently from other REEs. Europium may be found in a 2+ (in silicate minerals) or 3+ valency and will also behave differently from other REEs in solution. In the lanthanide series, the ionic radii and most complexation/stability constants vary systematically with increasing atomic number (Cantrell and Byrne, 1987; Byrne and Kim, 1990). The vertical distribution of dissolved REEs in a seawater column is relatively well characterized and is similar to the Si profile. These rather uniform profiles reflect differences in the individual REE chemical

properties upon interaction with particles, regeneration, scavenging, and adsorption (De Baar et al., 1983, 1985, 1988; Elderfield and Greaves, 1982; Klinkhammer et al., 1983; Piepgras and Jacobsen, 1992; Sholkovitz et al., 1994; Tachikawa et al., 1999; Alibo and Nozaki, 1999, 2000; Nozaki et al., 1999; Nozaki and Alibo, 2003).

In the hope that the differential geochemical properties of REEs can help constrain the behavior of settling particles, researchers have performed various pertinent studies (Murphy and Dymond, 1984; Fowler et al., 1992; Tachikawa et al., 1997; Lerche and Nozaki, 1998; Otosaka and Noriki, 2000). Nevertheless, spatial and temporal variations in REE patterns in settling particles are relatively small and random and have scarcely been understood in terms of the dynamic roles of settling particles in ocean chemistry. Lerche and Nozaki (1998) described differences in the REE signatures of three chemically different fractions after sequential leaching of settling particles. Otosaka and Noriki (2000) discussed compositional variations among REEs in settling particles in an attempt to elucidate the sources of REEs. Some researchers have used the REE composition of settling particles to calculate the REE flux in seawater using a mass balance approach (Murphy and Dymond, 1984; Fowler et al., 1992).

An interesting aspect of REEs in settling particles is the significant exchange of REEs between seawater and the labile components of settling particles, as discovered by Tachikawa et al. (1997, 1999) using Nd isotopes. This reaction was recently supported by model simulations (e.g., Arsouze et al., 2009). Common features of the REEs so far observed in settling particles are their enrichment in REEs, especially lighter REEs (LREEs), and their positive Ce anomalies relative to the ambient dissolved seawater phase. These are similar to features observed for suspended particles collected on 0.4 μm pore-sized filters (Sholkovitz et al., 1994). Particulate phases in seawater columns often show an increase of REE concentration with depth（Bertram and Elderfield, 1993; Sholkovitz et al., 1994）. The question is how to explain the increasing concentration of dissolved REEs with depth, which does not “mirror” (inverse relationship) the particulate REE profiles. Marine chemists have so far answered the question by ascribing it only to the release of REEs from a particulate oxide phase (for example, Sholkovitz et al., 1994).

In this paper, we report a dynamic aspect of settling particles and demonstrate the relationship that a “mirror-image process” is operative between REEs in solution and in a siliceous phase of suspended particles through diatom dissolution.

Methods

Settling-particle sampling

Sediment traps were deployed in two distinctly different subarctic environments (Fig. 1): Station SA, centrally located at a subarctic pelagic station (49°N, 174°W; water depth 5406 m), and Station AB, located at a marginal sea station (53.5°N, 177°W; water depth 3788 m). A PARFLUX-type sediment trap with 13 sample cups was tethered 600 m above the seafloor from August 10, 1995 to July 17, 1996 at Station SA and from August 7, 1995 to June 27, 1996 at Station AB (Takahashi et al., 2002). Station AB is characterized by a highly siliceous water column and sediments. Indeed, the highest dissolved silica concentration in the world (240 μmol/l) was measured in Bering Sea bottom water (Edmond et al., 1979; Tsunogai et al., 1979), and the Bering Sea is one of the most biologically productive areas in the world (Sambrotto et al., 1984). In contrast, the water of Station SA is less productive and the opal flux at this station is about half that of Station AB (Takahashi et al., 2000, 2002; Ashahi and Takahashi, 2007; Onodera and Takahashi, 2009).

The trap samples were fixed in situ with 5% formaldehyde buffered to pH 7.6–8.0 with sodium borate. The recovered samples were frozen onboard ship and thawed in port. Apparent swimmers were removed by hand-picking under a microscope when the original samples were split in port immediately after the trip. The swimmers were further removed by sieving through a 1000-μm mesh net. A subset of the samples were subjected to routine analysis for opal, calcium carbonate, and organic carbon contents (Takahashi et al., 2000).

REE determination (Fig. 2)

Bulk samples: A 256^{th} aliquot of the stored and sieved sediment trap suspension was centrifuged at 10^3 Gs for 10 min. The supernatant was removed and the residue was again centrifuged with 15 ml of ethanol for 10 min. The supernatant was removed and the residue was transferred to a PTFE beaker with a small volume of water, heated to dryness on a hot plate, and weighed. The residue was then digested with a mixture of 6 M HNO_3 (1 ml), 40% HF (1 ml), and 60% $HClO_4$ (0.5 ml). The digested liquid was evaporated to dryness and dissolved in 6 M HNO_3 and Milli-Q water. The final solution was subjected to REE separation to remove alkaline elements, whose presence might affect the accuracy of later spectrometric measurements. The REE separation procedure

was based on that of Shabani et al. (1990) and Fu et al. (1997, 1998). Briefly, the pH of the digested solution was adjusted to 2.4 ± 0.1 with an ammonia solution. The solution was transferred to a separating funnel to which 5 ml of a 0.25 M heptane solution of HDEHP (bis[2-ethylhexyl] phosphate) and H_2MEHP (2-ethylhexyl phosphate) mixture was added. REE chelates were preconcentrated in the heptane solution, then further treated with 0.1 M HNO_3 to remove any remaining matrix elements and with 5 ml of 6 M HCl to back-extract the REEs. The back-extraction procedure was repeated three times. The combined HCl solution was evaporated to dryness and dissolved in HNO_3 with a known amount of In as an internal standard. The accuracy of the solvent extraction was checked against a limestone geological standard (Ls-1) issued by the Geological Survey of Japan, but was not checked against seawater (Igarashi et al., 2003).

Siliceous fractions: A 256th aliquot of the stored and sieved sediment trap suspension was centrifuged for 10 min. The supernatant was removed and the residue was again centrifuged with 15 ml of ethanol for 10 min. The supernatant was removed and the residue was treated with 40% acetic acid for 10 min to remove the carbonate and reactive oxide phases (Sholkovitz et al., 1994). The acetic acid-soluble fraction should contain a relatively higher amount of interfering alkaline earth elements, which requires REE separation prior to the ICP-MS measurement. The available sample size (1/256 portion, typically 10 mg in dry weight) with a low carbonate content (typically 10 %) was too small to apply the REE separation without risking contamination. We did not analyze the acetic acid-soluble fraction. The solution was filtered through a Nuclepore filter (pore size 0.4 μm). We defined the fraction recovered on the filter as the "siliceous fraction," as this fraction should consist mainly of siliceous matter, but it may also contain other relatively refractory matter such as well-crystallized oxides and organic matter. We used acetic acid to compare our results with those of Lerche and Nozaki (1998). The filter was digested in a manner similar to that for bulk samples. The REE concentrations in the final HNO_3 solution were measured as described below. The solvent-extraction was not applied to the siliceous fractions, as the concentration of problematic alkaline earth elements were low in this fraction and BaO interference was corrected for as described later. A new filter was also analyzed in the same manner to evaluate the filter blank, which accounted for only 10% of the REEs in the specimen with the lowest concentration; no correction was made for the filter blank.

REE measurement: REEs in the solutions were determined by inductively coupled

plasma mass spectrometry (ICP–MS) at mass numbers La 139, Ce 140, Pr 141, Nd 146, Sm 147, Eu 151, Gd 157, Tb 159, Dy 162, Ho 165, Er 166, Tm 169, Yb 174, and Lu 175. Barium was also monitored because BaO interferes with Eu (Dulski, 2001; Igarashi et al., 2007); the influence of Ba and four LREEs (La, Ce, Pr, and Nd) was corrected using an oxide-forming factor obtained by measuring a solution containing these elements.

Sequential treatment for Mn, Fe, and Al determination

Acetic acid leaching cannot dissolve some well-crystallized oxides (Schwertmann, 1991; Raiswell et al., 1994) and we employed a modified procedure to see how effectively the acetic acid leaching treatment had removed the oxide fraction. A 1024^{th} aliquot was subjected to the same acetic-acid treatment used to isolate the siliceous fractions. The acetic acid solution was recovered by centrifugation into a PTFE beaker, evaporated to dryness on a hot plate, dissolved with 6 M HNO_3, and diluted with Milli-Q water to 10 ml of 0.1 M HNO_3 solution (acetic acid-soluble). The residue was treated with 10 ml of 0.1 M HCl at 60˚C for 20 min in a water bath. The solution was transferred to a PTFE beaker, evaporated to dryness on a hot plate, dissolved with 6 M HNO_3, and diluted with Milli-Q water to 10 ml of 0.1 M HNO_3 solution (HCl-soluble). The residue was transferred to a PTFE beaker, decomposed with a mixture of 6 M HNO_3 (1 ml), 40% HF (1 ml), and 60% $HClO_4$ (0.5 ml), evaporated to dryness, dissolved with 6 M HNO_3, and diluted with Milli-Q water to 10 ml of 0.1 M HNO_3 solution (HF-soluble). Mn, Fe, and Al in the solutions (i.e., acetic acid-soluble, HCl-soluble and HF-soluble) were determined by ICP atomic emission spectrometry (ICP–AES). The calibration was made using standard solutions and the detection limits of Mn, Fe, and Al are 1, 10, and 50 μg/g sample. The procedure blank was estimated by performing the same procedure without sample and the data was thus corrected.

Results

Tables 1 and 2 summarize the analytical results for REEs in the untreated bulk samples and the treated siliceous fractions at the two stations. The component data for settling particles and some additional basic data (Asahi and Takahashi, 2007) are also shown in Table 1. Figures 3 and 4 show the shale-normalized REE patterns of the bulk samples and siliceous fractions, respectively. The bulk samples and siliceous fractions show consistent and similar patterns, characterized by heavier REE enrichment

compared with shale. For both the bulk samples and the siliceous fractions, there is a slight kink around Gd and the profile flattens out for the middle and heavier REEs. The most conspicuous difference between them is that the bulk samples show negative Ce anomalies, whereas the siliceous fractions show small positive anomalies. In addition, the bulk samples have higher slopes in the LREE region of the pattern and less consistent Eu anomalies than the siliceous fractions. These differences can be ascribed mainly to the presence of carbonate and oxides in the bulk samples. Differences between some pairs (bulk – siliceous fraction) of samples are negative, indicating heterogeneity between the bulk sample and siliceous fraction aliquots and/or analytical uncertainties associated with the solvent extraction procedure applied to the bulk samples. The REE patterns of the average of differences (bulk – siliceous fraction) are shown in Fig. 5. The patterns are similar for Stations AB and SA, but the absolute concentrations for Station SA are 2 to 3 times larger than for Station AB.

To quantitatively discuss the REE patterns, we introduce four features of the REE pattern: Ce anomaly, Eu anomaly, ΣREE, and HREE index. The Ce and Eu anomalies indicate the extent of deviation from their neighboring elements in a logarithmic-scaled REE pattern. Higher (lower) anomaly values indicate either stronger (weaker) positive anomalies or weaker (stronger) negative anomalies. ΣREE is the sum of the fourteen REE concentrations (ng/g). The HREE index represents the extent to which the four heavier elements are enriched relative to their shale values. Values for the four features are listed in Tables 1 and 2.

Bulk samples: Clear differences in some features are noticeable between the two stations. The Ce anomaly at Station AB is higher (i.e., weaker negative Ce anomaly) than at Station SA and the ΣREE at Station AB is lower than at Station SA. Some features for the bulk samples correlate weakly with the proportions of opal and carbonate. The Ce anomaly correlates positively with the proportion of opal ($r = 0.77$, $p < 0.01$) and negatively with that of carbonate ($r = -0.80$, $p < 0.01$); the HREE index correlates positively with the proportion of opal ($r = 0.72$, $p < 0.01$) and negatively with that of carbonate ($r = -0.60$, $p < 0.01$); ΣREE correlates negatively with the proportion of opal ($r = -0.64$, $p < 0.01$) and positively with that of carbonate ($r = 0.62$, $p < 0.01$). Some features seem to be affected by the total mass and opal fluxes, but not by the carbonate flux. Specifically, all four features converge to fixed values with increasing total mass flux, whereas the Ce anomaly sharply decreases, ΣREE increases, and the Eu anomaly and HREE index scatter with decreasing total mass (Fig. 6).

Siliceous fractions: As with bulk samples, clear differences in some features are again noticeable between the two stations. The siliceous fraction at Station AB is characterized by a relatively higher Eu anomaly and HREE index and by a lower Ce anomaly and ΣREE than at Station SA. The siliceous fraction mainly contains opal and aluminosilicate. Although the residue values in Table 1 carry large errors, the Ce anomaly, HREE index and ΣREE for the siliceous fractions do not correlate significantly with opal/(opal+residue) (figure not shown), indicating that opal cannot be distinguished from the residue by either Ce anomaly, HREE index or ΣREE or that some minor components in the fraction may be responsible for the values. (It will be shown later that the original correlation is likely to have been modified by the preferential dissolution of elements in the particles.) Similar to the bulk samples, all four features converge to fixed values with increasing total mass flux (Fig. 7). The convergence values for the bulk samples and siliceous fractions are similar: the HREE index approaches 2.2±0.18 (calculated using data from the three highest total mass fluxes) and ΣREE approaches 5600±1600. Conversely, the convergence values for the Ce anomaly (0.83±0.05 for the bulk sample, 1.01±0.04 for the siliceous fraction, calculated for the three samples) differ noticeably between the two solid fractions.

Mn, Fe, and Al: Table 3 lists the concentrations of Mn, Fe, and Al in three different fractions of four settling-particle samples. The four samples were chosen as representative of settling particles collected during relatively low and high primary production months at both stations (AB6#5 and SA7#8 represent a low productivity month; AB6#9 and SA7#4 a high productivity month). The highest concentration of Fe was detected in the HF-dissolved fraction, and is essentially proportional to the concentration of Al, which is at the sub-percent level—much lower than the levels detected in settling particles studied by Otosaka and Noriki (2000). With the exception of sample AB#6, the highest productivity sample analyzed, the highest concentration of Mn was detected in the acetic acid-soluble fraction, and the smallest concentration was detected in the HCl-soluble fraction, indicating that acetic acid treatment thoroughly dissolves the Mn oxide fraction. A significant amount of Fe in the HCl-soluble fraction implies its partial release from clays or the presence of refractory iron oxides in the residue of the acetic acid treatment (Raiswell et al., 1994).

Discussion

Comparison of the REE patterns with those of previous studies

A few previous reports on REE composition in settling particles show some similarities and differences with the results of our study, although direct comparison is sometimes difficult because of differences in the methods used. Lerche and Nozaki (1998) and Otosaka and Noriki (2000) collected settling particles from the Japan Trench and reported similar general compositional patterns: an increase with increasing atomic number in the LREE region and a slight kink at Eu or Gd. In contrast, Tachikawa et al. (1997) reported that REE abundance patterns decrease with increasing atomic number in settling particles of the tropical Atlantic Ocean.

We attribute the negative Ce anomalies that we observed in bulk samples to the carbonate or oxide phase leached by acetic acid (see Fig. 5), and they correspond to the negative Ce anomaly of the acetic acid-soluble fraction observed by Lerche and Nozaki (1998). We also leached samples with acetic acid, but did not analyze the leachate for reasons stated in the Method section. The difference between our bulk and siliceous fractions (Fig. 5), which corresponds to the acetic acid-soluble fraction, shows a very similar pattern to that of the acetic acid-soluble fraction of Lerche and Nozaki (1998) with middle REE enrichment and a negative Ce anomaly. Nevertheless, our inferred acetic acid-soluble fraction (bulk - siliceous fraction) shows a negative Eu anomaly, but their patterns do not. This is probably due to BaO interference in their data, as they did not isolate the REEs before analysis. A higher REE content at Station SA than at Station AB is roughly consistent with the higher proportion of $CaCO_3$ at Station SA (average = 29.3%) than at Station AB (average = 12.4%). The middle REE enrichment that we observed in bulk samples simply reflects the presence of a carbonate phase enriched in middle-REEs in the acetic acid-soluble fraction (Akagi et al., 2004; Palmer, 1985). As we did not perform REE separation on the siliceous fractions, the sum of the $HCl+HNO_3$-leached and residue fractions obtained by Lerche and Nozaki (1998) corresponds to our siliceous fractions and, in general, shows very similar patterns. The most striking observation reported by Lerche and Nozaki (1998) is the marked positive Ce anomaly, as high as 10, observed in their residue after the $HCl+HNO_3$ leaching treatment. We also observed positive Ce anomalies in our siliceous fractions, and a possible explanation for the Ce anomaly is presented later.

Mixing as an explanation for variations in the bulk REE signature

The observed correlations between the REE signatures and opal and carbonate

contents of the bulk samples (correlation factors mentioned in “Results” section, figure not shown) may be interpreted as the REE signatures of opal and carbonate: (1) opal and carbonate are major carriers of HREEs and LREEs, respectively; (2) opal has a weaker Ce anomaly and a lower ΣREE than carbonate and displays HREE enrichment; (3) conversely, carbonate has a stronger negative Ce anomaly and a higher ΣREE than opal and displays LREE enrichment. The concentration of Mn in the acetic acid-soluble fraction also correlates with the Ce anomaly, HREE index and ΣREE of the bulk samples. The observed negative correlation of Mn concentration with Ce anomaly is difficult to explain by the presence of Mn oxide phases alone and the Mn concentration in the acetic acid-soluble fraction is not high enough to explain the REE concentration in the leach (e.g., Mn 170 μg/g and ΣREE 10 μg/g in sample SA7#8). We consider that Mn oxide phases play a secondary role relative to carbonates. Biogenic carbonate may have a lower ΣREE and display a slight HREE enrichment with respect to seawater (Akagi et al., 2004; Sholkovitz and Shen, 1995), but inorganic carbonates are believed to have a high ΣREE with LREE enrichment (Zhong and Mucci, 1995; Scherer and Seita, 1980; Rimstidt et al., 1998). Because Ce does not partition anomalously in carbonates from seawater, the carbonate phase mirrors the Ce anomaly of REEs dissolved in seawater. No direct measurement of diatoms has been reported to date, but, as discussed later, opal is thought to have a lower REE content with a highly HREE-enriched pattern. Initially, the idea that diatoms are a major carrier of HREEs seemed improbable, because both the HREE concentration and ΣREE are negatively correlated with opal content, but we will return to this idea later in the Discussion.

The hyperbolic relationship shown in Fig. 6 is usually explained by the dilution of one component by another. A similar relationship exists between the REE pattern features and the total mass flux, the opal flux, and even the amount of residue, but not the carbonate flux. We therefore conclude that one component is a carbonate and that the hyperbolic curves indicate the dilution of the REE signature of the carbonate by opaline matter. A hyperbolic fit to the relationship (Fig. 8) suggests that the carbonate has a ΣREE greater than 5 mg/g and a Ce anomaly of less than 0.5. It has been reported that the distribution factor of REEs in inorganic carbonate is on the order of 10^3 (Zhong and Mucci, 1995). The concentration of La in the acetic acid-soluble fraction (= bulk – siliceous fraction) is correlated with the proportion of $CaCO_3$ ($r = 0.55$, $p<0.01$, figure not shown). From the slope of the correlation, the distribution factor between settling particles and seawater of a similar depth (Alibo and Nozaki, 1999) is in the range of 10^2

to $4x10^3$, supporting the hypothesis that the REEs are associated mainly with inorganic carbonate.

We examined the data for the acetic acid-soluble phase of settling particles reported by Lerche and Nozaki (1998) and discovered that the REE distribution pattern between this phase and seawater is fairly similar to that between the acetic acid-soluble phase of suspended particles (collected on filters) and seawater reported by Sholkovitz et al. (1994) (Fig. 9). The distribution pattern is characterized by a LREE enrichment and a marked positive Ce anomaly. The Ce anomaly (Ce/Ce*) in the distribution patterns ranges from 10 (Sholkovitz et al., 1994) to 100 (Lerche and Nozaki, 1998). Since the REEs in our "inferred" acetic acid-soluble fraction correlate with the carbonate content of sediment trap material, the LREE enrichment in Fig. 9 may be due to the preferential partitioning of LREEs between inorganic carbonate and seawater, as reported by Zhong and Mucci (1995). The strong positive Ce anomaly seen in Fig. 9, however, cannot be explained by the inorganic carbonate component. As stated earlier, the acetic acid-soluble fraction is a major carrier of Mn, whose oxide can selectively oxidize Ce(III) to Ce(IV) and thus immobilize the element (Ohta and Kawabe, 2001). We believe that the presence of Ce in the acetic acid-soluble fraction may be a result of preferential oxidative adsorption of Ce on the Mn oxide. Although the Mn concentration in the acetic acid-soluble fraction correlates negatively with the Ce anomaly of our bulk samples, the Ce concentration in particles seems to correlate largely with the Mn concentration. In fact, the "excess-Mn", which cannot be explained by the presence of clay using the data reported for the settling particles in the Japan Trench (Otosaka and Noriki, 2000) and the upper crustal data (Rudnick and Gao, 2003) as a proxy of clay composition, was much higher than that observed in our acetic acid-soluble fraction. Using the excess-Mn data and the amount of the acetic acid-soluble Ce measured by Lerche and Nozaki (1998), we calculated the ratios of Ce/Mn in the acetic acid-soluble phases of settling particles in the Japan Trench and found that the ratios always fall between 0.005 and 0.02 for both the settling and suspended particles (collected on filters, Sholkovitz et al., 1994). The negative Ce anomaly in our acetic acid-soluble phase may simply reflect both a negative Ce anomaly of the dissolved REEs in the ambient seawater (likely <0.1 according to De Baar et al., 1985; Lerche and Nozaki, 1998) and a much smaller amount of Mn in our acetic acid-soluble phase.

The measurement of Eu is subject to spectral overlapping with BaO, which might be more serious at low REE concentrations (Dulski, 2001; Igarashi et al., 2007).

375 Nevertheless, the large scattering of the Eu anomaly and HREE index at low total mass
376 flux is not likely to be an analytical artifact, but seems difficult to explain. Lerche and
377 Nozaki (1998) reported a negative Ce anomaly in their acetic acid-soluble fraction.
378 Because their acetic acid-leach fraction accounted for only about 10% of the REE
379 amount in their settling particles, the bulk settling particles exhibited positive Ce
380 anomalies. In contrast, our "inferred" acetic acid-soluble fraction represents a
381 significant proportion of the bulk samples, and the bulk samples show negative Ce
382 anomalies. The asymptote of the fitting curve in Fig. 8 indicates that the Ce anomaly is
383 negative, whereas no Ce anomaly is seen in the asymptote of the siliceous fractions, as
384 discussed later. The difference in Ce anomaly between the two asymptotes is explained
385 by the presence/absence of a carbonate phase with a negative Ce anomaly at about 10%
386 weight of opal.
387
388 *Diatom contribution to the siliceous fraction*
389 The Si/Al ratios of the siliceous fraction for the four samples in Table 3 range
390 from 27.4 (SA7#4) to 65.6 (AB6#9), which are much higher than the average ratio of
391 8.5 for the settling particles collected by Otosaka and Noriki (2000) and of clay (4.0,
392 Otosaka and Noriki, 2000). The greater contribution of opal to the settling particles is
393 due to the high productivity of the area. The La/Al ratios ($2.3\text{-}3.9\times10^{-4}$) are the upper
394 crust value (3.8×10^{-4}; Rudnick and Gao, 2003), whereas the Lu/Al ratios ($5.2\text{-}9.7\times10^{-6}$)
395 are higher than in the upper crust (3.8×10^{-6}) with the ratio for the sample with the
396 smallest opal flux being exceptionally low (5.2×10^{-6}). This indicates the existence of
397 excess HREEs, which cannot be explained by the presence of aluminosilicates. Neither
398 selective adsorption of HREEs to, nor selective desorption of LREEs from silicate
399 phases can be responsible for HREE enrichment in solid silicate phases according to the
400 experiments of Byrne and Kim (1990). It is considered that HREE enrichment is a result
401 of high diatomaceous contribution. The HREE index of the siliceous fraction ranges
402 from 1.64 to 2.95 with the average being 2.08. In comparison, the HREE index of the
403 upper crust is 0.92 (Rudnick and Gao, 2003) and that of 42 Chinese airborne samples
404 varies from 0.63 to 1.81 with the average being 1.16 (Yang et al., 2007). The mineral
405 residue obtained by a sequential acetic acid, sodium carbonate, and sodium dithionite
406 treatment of sediment from the Northwest Pacific Ocean show HREE index values as
407 high as 2.58 (Nakai et al., 1993), which the authors interpreted as being characteristic of
408 the local dust. The high HREE index of our settling particles alone, therefore, could not

409 be considered as solid evidence for diatom contribution. Considering the high Si/Al and
410 Lu/Al ratios of our siliceous fractions, we conclude that the siliceous fraction with the
411 higher HREE index has a significant diatom contribution and that significant HREE
412 enrichment may be a characteristic feature of diatom REEs.
413 The Lu/Si ratio of the siliceous fraction ranges from $6x10^{-8}$ to $3.4x10^{-7}$ with
414 an average of $1.5x10^{-7}$. The smallest ratio is observed for the sample with the highest
415 opal mass flux (AB6#10), and is considered to be closest to the characteristics of
416 diatoms, an interpretation that will be further justified in terms of dissolution dynamics.
417 As discussed later, the ratio is almost identical to the concentration ratio of deep ocean
418 water. Since diatoms are an important carrier of Si in the seawater column (Redfield et
419 al., 1963), the present set of data indicates that diatoms must be considered as an
420 important carrier of HREEs in a seawater column.
421
422 *Problems in explaining the variations in the REE signatures of the siliceous fractions by*
423 *mixing*
424 Station AB is located in the Bering Sea Gyre and Station SA is in the open
425 subarctic Pacific. Station SA is influenced by two surface currents flowing in opposite
426 directions: the Subarctic Current and the Alaskan Stream (Asahi et al., 2007). One of the
427 present authors reported that the dynamics of settling particles at Stations AB and SA
428 may be controlled by the two water currents, which are rather independent of each other
429 (Onodera and Takahashi, 2009). One may be inclined to consider that the differences in
430 the features of the REE patterns for the siliceous fraction between the two stations may
431 simply reflect the difference of water masses and/or circulation. For example, water of
432 Station AB is characterized by a lower REE concentration, a weaker positive Ce
433 anomaly, and a greater HREE enrichment than that of Station SA. The higher
434 productivity of Station AB is due to more vigorous mixing of the subsurface layer, into
435 which the nutrient-rich deep water of North Pacific flows (Tsunogai et al., 1979). The
436 REE signatures of the deep North Pacific water (a high ΣREE with a strong negative Ce
437 anomaly, De Baar et al., 1985; Piepgras and Jacobsen, 1992; Alibo and Nozaki, 1999)
438 conflict with this interpretation. We consider that the water mass difference does not
439 account for the variations in the REE signatures.
440 We then checked whether different REE signatures from different sources
441 could explain variations and correlations among them. Geochemically important
442 sources of REEs in the ocean include opal particles, calcite particles, airborne particles,

443 and deeper water. Each has a different REE signature: no direct measurement of diatoms
444 has been reported yet, but diatoms have been shown to consistently have an
445 HREE-enriched pattern (see earlier and later in the discussion); calcite has an
446 HREE-enriched pattern with a Ce anomaly (Akagi et al., 2004; Palmer, 1985); airborne
447 particles have a relatively flat REE pattern with higher REE abundance than opal (Nakai
448 et al., 1993; Yang et al., 2007); and deep ocean water is characterized by a strong
449 negative Ce anomaly and HREE enrichment (De Baar et al., 1985; Alibo and Nozaki,
450 1999). Nevertheless, no combination of the four sources can consistently explain the
451 variations and correlations observed in this study. For example, the lower HREE index
452 and higher ΣREE values in Fig. 7 may be explained by a greater contribution of REEs
453 from airborne particles, but the stronger negative Ce anomaly remains unexplained.
454 Similarly, the stronger negative Ce anomaly may be explained by contributions of either
455 carbonate particles or upwelling water, but the lower HREE index remains unexplained.
456 Therefore, we have rejected the idea of mixing REEs from different sources.
457 Similar to the case for the bulk samples (Figs. 6 and 8), a hyperbolic
458 relationship can be seen with the total mass (Fig. 7 e, f, g and h), as well as the opal flux
459 (Fig. 7 a, b, c and d), carbonate flux (not shown), and residue (or Al) amount (not
460 shown) of the settling particles. If these relationships can be explained by mixing, there
461 should be an end-member in the siliceous fractions which is concentrated in REEs, with
462 a positive Ce anomaly, a negative Eu anomaly, and a relative enrichment in LREEs, all
463 of which become more pronounced with decreasing amounts of settling particles, and
464 another end-member as a diluent. Mn/Fe oxide may be a candidate for the source of
465 concentrated REEs. Sholkovitz et al. (1994) observed a positive Ce anomaly and
466 enrichment of LREE in oxide phases, but our siliceous fractions are not major carriers
467 of Mn oxide (Table 3). They contain most of the Fe, whose concentration maintains a
468 1:2 proportional relationship with Al, almost identical to that of the average crust
469 (Rudnick and Gao, 2003). Most of the Fe in the siliceous fractions is considered to be in
470 the form of aluminosilicate. As shown in Table 3, a significant amount of Fe was
471 detected in the HCl-soluble fraction. The presence of well-crystallized Fe oxides in the
472 siliceous fraction is possible and this phase may be responsible for the concentrated
473 REEs. Even if we allow for the existence of such a REE-enriched end-member, we then
474 have a problem with a diluent. Aeolian dust with a relatively high HREE index (Nakai
475 et al., 1993) is not appropriate, if we consider the extremely high Si/Al ratio and low
476 REE concentration of the siliceous fraction at a higher mass flux. One of the most

plausible combinations to generate a parabolic relation is refractory Fe oxides as the REE-enriched end-member and opal as a diluent, but the observed LREE enrichment is difficult to reproduce from dissolved REEs in seawater using any distribution factors for $Fe(OH)_3$ phases (Bau, 1999; Ohta and Kawabe, 2000).

As discussed later, another explanation based on the differential dissolution kinetics of elements in siliceous matter seems to provide a much more reasonable picture of the REE behavior of settling particles.

Dissolution to produce variations in the REE patterns of settling particles

Fowler et al. (1992) analyzed bulk settling particles and observed that the extent of LREE enrichment and positive Ce anomaly decreases after a phytoplankton bloom. They proposed that REE fractionation may be kinetically controlled, with fast-sinking particles leading to less fractionation. Our observation is that, at higher mass flux, the settling particles show a greater HREE enrichment and a weaker positive Ce anomaly. Fowler et al.'s (1992) observations and interpretation are similar to ours and we will develop a kinetic model to explain the fractionation. One can explain fractionation in two different ways: absorption and dissolution. Based on our results, the development of a positive Ce anomaly and LREE enrichment in the siliceous fraction can be explained by their preferential adsorption. Nevertheless, we considered it better to explain the same fractionation by preferential dissolution of Si and HREEs for the following reasons: 1) the siliceous fractions are not major carriers of Mn (Table 3), 2) Si is readily recycled in most of water columns (Nelson et al., 1995), and 3) LREEs are not preferentially adsorbed onto silicate phases (Byrne and Kim,1990).

At higher particle densities, particles tend to aggregate and settle faster, reducing the time available for REEs to dissolve. Aggregated particles also have less surface area per unit mass than before aggregation. Consideration of dissolution dynamics leads to the following formulas linking the dissolution rate of particles and productivity (see Appendix).

$$\sum \mathrm{REE} \approx C^{o}_{\mathrm{REE}}\left[1+\frac{(k_{\mathrm{LREE,\,MREE}}-k_{\mathrm{Si}})fD}{P^2}\right], \qquad (1)$$

$$\mathrm{Ce\ anomaly} \approx \mathrm{Ce\ anomaly}^{o}\left[1+\frac{(k_{\mathrm{Ce}}-k_{\mathrm{LREE}})fD}{P^2}\right], \qquad (2)$$

$$\mathrm{Eu\ anomaly} \approx \mathrm{Eu\ anomaly}^{o}\left[1+\frac{(k_{\mathrm{Eu}}-k_{\mathrm{MREE}})fD}{P^2}\right], \text{ and} \qquad (3)$$

$$\text{HREE index} \approx \text{HREE index}^{\circ}\left[1+\frac{(k_{\text{HREE}}-k_{\text{LREE}})fD}{P^2}\right], \quad (4)$$

where f is a conversion factor between two proportionality constants (see Appendix), k_i is the specific dissolution rate of element i, D is the vertical distance that particles travel from the surface ocean, and P is the particle density. Superscript "O" indicates initial values before settling. The simulated plots in the Appendix show that differences in sampling depths and in the weight of particles between the surface and the sampling depth may cause only minor differences in fitting. Therefore, we neglected the sampling depth difference between the two stations (Station SA, 4806 m; Station AB, 3188 m) and adopted the flux data recorded at the sampling depths as the initial particle density before settling. By fitting, one can only estimate the numerator values in Eqs (1) to (4) and absolute values of the parameters cannot be estimated.

The observed relationships of the REE features of the settling particles to the opal flux shown in Fig. 7 a, b, c and d were fitted to the above functions. Opal flux instead of the particle density in the surface water was used in the equations for the following reasons: (1) it is the dominant component of settling particles; (2) it is a direct proxy of primary production; and (3) diatoms may act as an adhesive agent for aggregations, unlike carbonate (Kiorboe, 1997). The fitting results are shown in Fig. 10. All the relationships appear to be fairly well fitted by Eqs (1) to (4), considering that naturally-occurring variations and mixing of differently-aggregated particles are neglected in the model (see Appendix). Using the total mass of settling particles instead of the opal flux as a proxy for the particle density gives very similar plots to those shown in Fig. 10, which makes no difference to the following discussion. From the fit, we obtain the following range of values:

$$(k_{\text{LREE, MREE}}-k_{\text{Si}})fD \approx \left(1\times10^{3}\right)\sim\left(8\times10^{3}\right) \quad (5)$$

$$(k_{\text{Ce}}-k_{\text{LREE}})fD \approx \left(1\times10^{2}\right)\sim\left(8\times10^{2}\right) \quad (6)$$

$$(k_{\text{Eu}}-k_{\text{MREE}})fD \approx \left(-1\times10^{2}\right)\sim\left(-1.5\times10^{3}\right) \quad (7)$$

$$(k_{\text{HREE}}-k_{\text{LREE}})fD \approx \left(-2\times10^{2}\right)\sim\left(-1.5\times10^{3}\right) \quad (8)$$

Although the calculations carry large uncertainties, the computed values in Eqs. (5) to (8) are quite different from one another. Most thermodynamic constants change monotonously over the whole range of REEs (Cantrell and Byrne, 1987; Byrne and Kim, 1990) and, if MREE dissolves at a rate midway between LREE and HREE, we obtain the following order of dissolution rates from the settling particles.

$$\text{Ce} < \text{LREEs} < \text{MREEs} < \text{Eu} \approx \text{HREEs} < \text{Si} \quad (9)$$

The relative dissolution rates among the REEs are supported by variations in the REE pattern of the siliceous fractions: when the patterns are viewed after the La data are normalized to unity (figure not shown), they monotonously increase with increasing atomic number except for Ce.

Vertical profiles of dissolved REEs explained by their differential dissolution rates from settling particles

The vertical profiles of dissolved REEs in a seawater column have been explained in terms of scavenging of REEs by particles at the surface and subsequent release from particles in deeper water (Byrne and Kim, 1990; Sholkovitz et al., 1994; Oka et al., 2009). The difference among individual REE profiles has been interpreted in terms of their differential distribution coefficients between particles and solution. The results of the present study and our interpretation of the results, however, strongly suggest that the siliceous fraction of settling particles is an important carrier of REEs in a seawater column. A new interpretation of the vertical profiles of REEs will be undertaken in this section.

The profiles of Piepgras and Jacobsen (1992) and Alibo and Nozaki (1999), in which the concentration of each REE increases almost monotonically with depth in the ocean, are chosen as typical examples. To ease comparison of the REE profiles, we normalized the profiles for all elements to vary between 0 and 1 (Fig. 11).

In both profiles, the four HREEs approach maximum concentrations at shallower depths, indicating a high HREE dissolution rate. The patterns of LREEs, MREEs, and Eu are hard to discern and La tends to differ slightly from other LREEs. The Ce profile is always anomalous and, with the exception of a surface peak, is rather randomly distributed; the concentration of Ce is more or less uniform with depth and the normalization of its concentration emphasizes the randomness. Piepgras and Jacobsen (1986) also reported dissolved Si concentrations and these are reproduced in Fig. 11 a and b. The lateral transport of deep water tends to decrease the concentration of REEs as well as Si. In other areas of the Pacific Ocean, the vertical profile of Si reaches a maximum at much shallower depths than do those of the REEs (Nozaki, 2001, Zhang et al., 1998). It is obvious that dissolution of biogenic silica is completed at much shallower depths than is the dissolution of REEs. If we assume that the depth profile is largely governed by the regeneration rate of each REE, the order would be

$$\mathrm{Ce} < \mathrm{LREEs} = \mathrm{MREEs} = \mathrm{Eu} < \mathrm{HREEs} < \mathrm{Si}. \quad (10)$$

Relations (9) and (10) differ in the order of MREEs and Eu between LREE and HREE. This difference can be explained by the absorption of REEs onto and dissolution of REEs from a carbonate phase. Biogenic carbonates are slightly enriched in MREEs (Akagi et al., 2004; Palmer, 1985). Enrichment of MREEs was observed in the "inferred" acetic acid-soluble phase of settling particles in this investigation (Fig. 5) as well as in an earlier study (Lerche and Nozaki, 1998). Qualitatively, in water above carbonate mineral saturation depths, carbonate acts as a carrier of MREEs. The MREEs can partially be released to the water column in calcite or aragonite undersaturated water, resulting in deepening of maximum concentration in their vertical profiles.

Another important feature to note is the ΔLu/ΔSi (the difference in the dissolved concentration between the surface and deep water for Lu divided by that for Si) in a seawater column. We selected Lu because it is the most soluble REE and it is most likely that the dissolution of all Lu from biogenic silica occurs well above the bottom in Fig. 11 a and b. This ratio is 4.8×10^{-8} to 6.5×10^{-8} according to Piepgras and Jacobsen (1988, 1992), almost identical to that of our *original* siliceous fraction (~6×10^{-8}). Hence, we concluded that dissolution dynamics provides a much better explanation for the REE variations in the siliceous fractions. Incidentally, the ΔLu/ΔSi ratio is much lower than the Lu/Si value of the upper crust (1.0×10^{-6}, Rudnick and Gao, 2003), which implies that diatoms are the exclusive carrier of HREEs in the ocean column and that airborne crustal material may not play an important role in supplying HREEs to deep water.

Estimation of the REE signatures for some components in the settling particles

The REE pattern of the bulk samples can be understood in terms of the relative contributions of the siliceous components and carbonate phase. The REE pattern of the former can vary due to dissolution and that of the latter due to adsorptive exchange with REEs dissolved in seawater, according to their respective partitioning factors (Fig. 9).

The asymptotes of the siliceous fraction (Fig. 10) must indicate the REE pattern of *original* siliceous matter, which has not experienced REE fractionation through dissolution. The asymptotic end-member values are 1.0 for the Ce anomaly, 1.2 for the Eu anomaly, around 5000–6000 for ΣREE, and 2–2.5 for the HREE index. These values are almost identical to the average for the siliceous fractions of AB-6#9 and AB-6#10 (Table 2). The proportion of opal in the siliceous fraction of the two samples

609 is >85% according to the results of our component analysis (Table 1), and the REE
610 parameters/features may be close to the diatom value. Considering the concentration of
611 Al in the siliceous fraction, most LREEs exist in aluminosilicates. The Lu/Si ratio of the
612 two samples (as low as $6x10^{-8}$) is much lower than that of clay ($1.0x10^{-6}$, calculated
613 using the upper-crustal values by Rudnick and Gao, 2003). Nevertheless, the high Lu/Al
614 and Lu/La ratios indicate that the contribution of aluminosilicates to HREEs in the
615 *original* siliceous matter may be smaller than that of diatoms. The HREE enrichment in
616 diatom silica shells is first reported in this study and the reason for the enrichment is
617 beyond the scope of the present study. Most ligands preferentially complex with HREEs
618 (Cantrell and Byrne, 1987; Byrne and Kim, 1990) and the complexation with the
619 transporter molecules of silica units identified in diatoms (Hildebrand et al., 1997) may
620 be one of the mechanisms responsible for the HREE enrichment.
621 Our conclusion that diatoms are a major carrier of HREEs seems to conflict
622 with the observation that the concentration of HREEs decreases with the increase of
623 opal flux as well as opal content in settling particles. Our dissolution model shows that
624 it does not conflict because 1) the higher HREE concentration results from the
625 progressive dissolution of silica and 2) the actual HREE flux, expressed by the product
626 of the HREE concentration and opal flux, increases with the increase of opal flux.
627 Fitting of a mixing model to the bulk samples (Fig. 8) indicates that the
628 carbonate phase has a Ce anomaly of 0.5 and a ΣREE of 0.5–1 mg/g, which is likely to
629 be representative of the authigenic inorganic carbonate.
630
631 *Explainable discrepancies in the reported REE patterns of settling particles*
632 Lerche and Nozaki (1998) measured REEs in three fractions from sequential
633 leaching of settling particles: acetic acid-soluble, $HCl+HNO_3$ acid-soluble, and HF
634 soluble residue. Our siliceous fractions correspond to the sum of their acid-leached
635 sample and residue. This is the rationale for plotting the sum of their data on Fig. 7 e, f,
636 g and h. Their data appear to form a similar hyperbolic trend, although they all plot in
637 an extreme region of the trend. We also include their values in Fig. 10. Unfortunately,
638 they did not report the opal abundance of their samples. Otosaka and Noriki (2000)
639 reported that opal accounted for an average of 30% of the settling particles collected
640 from the Japan Trench. From the relationship between the total mass flux and opaline
641 content in their study, we estimated an opal contribution of 20±10% for the settling
642 particles studied by Lerche and Nozaki (1998). Assuming that 20% of their particles

consist of opal, we plotted their data from 3680 m (the closest sampling depth to ours) (Fig. 10). Their data fall exactly along our fitting curves for the four features, indicating that their data, including the enigmatic positive Ce anomalies, should be explained by fractionation through the same dissolution kinetics: longer contact time with seawater due to lower productivity. In fact, their study area, compared to ours, is less productive. This consideration may validate the model developed in this study.

Conclusions

Two REE-enriched phases were identified in settling particles. One phase is likely a carbonate, which concentrates REEs according to their respective distribution factor in seawater. Oxides may not be important scavengers of REEs in the area studied. Another phase is associated with siliceous matter and may form by partial and preferential dissolution of Si. Siliceous matter is considered to originally be a mixture of LREE-enriched aluminosilicates and HREE-enriched diatoms. The higher HREEs/Al and Si/Al ratios of the siliceous matter reflect the potential importance of diatoms as carriers of HREEs in the oceanic water columns. By applying a kinetic model to the REE fractionation of siliceous matter, we compared the dissolution rate of each REE with its vertical profile in a seawater column. Dissolution kinetics explains why the vertical profiles of dissolved REEs are similar to that of Si. The Lu/Si ratio estimated for the original siliceous matter is comparable to that of the dissolved elements in deep water. The general picture of REE behavior in a seawater column inferred by this study is illustrated in Fig. 12. This will have to be tested against observations that the conventional scavenging mechanism has failed to explain.

The composition of the settling particles in areas of lower production tends to be subject to greater variations in both components, even though the mechanisms responsible for the variations differ: dissolution of the siliceous fraction and reactions with authigenic inorganic carbonates for the bulk. Such variations may have long hampered a systematic understanding of the compositional variation of settling particles (Anderson, 2006; Archer, 2006). The stations investigated in this study may be unique because diatomaceous productivity is much higher than in stations studied previously, which enabled us to observe much smaller compositional variations of settling particles from the original composition of diatoms.

Acknowledgement

We thank Dr Alfonso Mucci for the attentive editing and comments and three reviewers for the helpful comments. We would like to express our sincere thanks to the late Professor Yoshiyuki Nozaki. This research was initiated following his kind introduction of one of the coauthors (K. T.) to the lead author.

References

Akagi T., Hashimoto Y., Tao H., Tsuno H., Fu F-F. and Nakano Y. (2004) Variation of the distribution coefficients of rare earth elements in modern coral-lattices: species and site dependencies. *Geochim. Cosmochim. Acta.* **68**, 2265-2273.

Alibo D.S. and Nozaki Y. (1999) Rare earth elements in seawater: Particle association, shale-normalization, and Ce oxidation. *Geochim. Cosmochim. Acta*. **63**, 363-372.

Alibo D.S. and Nozaki Y. (2000) Dissolved rare earth elements in the South China Sea: Geochemical characterization of the water masses. *J. Geophys. Res.* **105**. 28771-28783.

Alldredge A.L. and Gotschalk C. (1988) In situ settling behavior of marine snow. *Limnol. Oceanogr.* **33**, 339-351.

Anderson R.F. (2006) Chemical tracers of particle transport. In: *Treatise on Geochemistry. Vol. 6 The Oceans and Marine Geochemistry. (*ed. H. Elderfield). Elsevier, pp. 247-273.

Archer D. (2006) Biological fluxes in the ocean and atmospheric p_{CO2}. In: *Treatise on Geochemistry. Vol. 6 The Oceans and Marine Geochemistry.* (ed. H. Elderfield). Elsevier, pp. 275-291.

Arsouze T., Dutay J.-C., Lacan F. and Jeandel C. (2009) Reconstructing the Nd oceanic cycle using a coupled dynamical-biogeochemical model. *Biogeosciences Discuss.* **6**, 5549-5588.

Asahi A. and Takahashi K. (2007) A 9-year time-series of planktonic foraminifer fluxes and environmental change in the Bering sea and the central subarctic Pacific Ocean, 1990-1999. *Progress in Oceanography* **72**, 343-363.

Bau, M. (1999) Scavenging of dissolved yttrium and rare earths by precipitating iron oxyhydroxide: Experimental evidence for Ce oxidation, Y-Ho fractionation, and lanthanide tetrad effect. *Geochim. Cosmochim. Acta* **63**, 67-77.

Berelson W.M. (2002) Particle settling rates increase with depth in the ocean. *Deep-Sea Res.* **49**, 237-251.

Bertram C.J. and Elderfield H. (1993) The geochemical balance of the rare earth

711 elements and neodymium isotopes in the oceans. *Geochim. Cosmochim. Acta* **57**,
712 1957-1986.
713 Brookins D. G. (1983) Eh-pH diagrams for the rare earth elements at 25 ºC and one bar
714 pressure. *Geochem. J.* **17**, 223-229.
715 Byrne R. H. and Kim K.-H. (1990) Rare earth element scavenging in seawater. *Geochim.*
716 *Cosmochim. Acta* **54**, 2645-2656.
717 Cantrell K.J. and Byrne R.H. (1987) Rare earth element complexation by carbonate and
718 oxalate ions. *Geochim. Cosmochim. Acta* **51**, 597-605.
719 De Baar H.J.W., Bacon M.P. and Brewer P.G. (1983) Rare-earth distributions with a
720 positive Ce anomaly in the Western North Atlantic Ocean. *Nature* **301**, 324-327.
721 De Baar H.J.W., Bacon M.P. and Brewer P.G. (1985) Rare earth elements in the Pacific
722 and Atlantic Oceans. *Geochim. Cosmochim. Acta.* **49**, 1943-1959.
723 De Baar H.J.W., German C.R., Elderfield H. and Gaans P.V. (1988) Rare earth element
724 distributions in anoxic waters of Cariaco Trench. *Geochim. Cosmochim. Acta*. **52**,
725 1203-1219.
726 Dulski P. (2001) Reference materials for geochemical studies: New analytical data by
727 ICP-MS and critical discussion of reference values. *Geostandard Newslett.* 25,
728 87-125.
729 Edmond J.M., Jacobs S.S., Gordon A.L., Mantyla A.W. and Weiss R.F. (1979) Water
730 column anomalies in dissolved silica over opaline pelagic sediment and the origin of
731 the deep silica maximum. *Jour. Geophys. Res.* **84**, 7809-7826.
732 Elderfield H., Hawkesworth C.J., Greaves M.J. and Calvert S.E. (1981) Rare earth
733 element geochemistry of oceanic ferromanganese nodules and associated sediments.
734 *Geochim. Cosmochim. Acta*. **45**, 513-526.
735 Elderfield H. and Greaves M.J. (1982) The rare earth elements in seawater. *Nature* **296**,
736 214-219.
737 Fowler S.W., Hamilton T.F., Peinert R.D., La Rosa J. and Teyssie J.-L. (1992) The
738 vertical flux of rare earth elements in the northwestern Mediterranean Sea. *Water*
739 *Pollut. Res. Rep.* **28**, 401-412.
740 Fu F-F., Shinozuka K., Ebihara M. and Akagi T. (1997) Distribution ratio of dissolved
741 and particulate REE in surface coastal seawater. *Geochem. J.* **31**, 303-314.
742 Fu F.-F., Akagi T. and Shinotsuka K. (1998) Distribution pattern of rare earth elements
743 in fern: implication for intake of fresh silicate particles by plants. *Biological Trace*
744 *Element Research*, **64**, 13-26.

745 Gnanadesikan A. (1999) A global model of silica cycling: sensitivity to eddy
746 parameterization and remineralization. *Global Biogeochem. Cycles* **13**, 199-220.
747 Goldstein S.J. and Jacobsen S.B. (1988) Rare earth elements in river waters. *Earth*
748 *Planetary Science Letters* **89**, 35-47.
749 Hildebrand M., Volcani B.E., Gassmann W. and Schroeder J.I. (1997) A gen family of
750 silicon transporters. *Nature* **385**, 688-689.
751 Honjo S. and Manganini S.J. (1993) Annual biogenic particle fluxes to the interior of N
752 Atlantic Ocean; studied at 34°N 21°W and 48°N 21°W. *Deep-Sea Res*. **40**, 587-607.
753 Honjo S., Dymond J., Collier R. and Manganini S.J. (1995) Export production of
754 particles to the interior of the equatorial pacific ocean during the 1992 EqPac
755 experiment. *Dep-Sea Res*. **42**, 831-870.
756 Honjo S. (1996) Fluxes of particles to the interior of the open oceans. In: *Particle Flux*
757 *in the Ocean* (eds. V. Ittekkot., P. Aschaufter, S. Honjyo, and P. Depetris) Wiley, New
758 York.
759 Honjo S., Dymond J., Prell W. and Ittekkot V. (1999) Monsoon-controlled export fluxes
760 to the interior of the Arabian sea. *Dep-Sea Res*. **46**, 1859-1902.
761 Igarashi K., Akagi T., Fu F.-F. and Yabuki S. (2003) Determination of rare earth
762 elements in a limestone geological standard using solvent extraction with ICP-MS
763 detection. *Anal. Sci.* **2003**, 441-445.
764 Kiorboe T. (1997) Small-scale turbulence, marine snow formation, and planktivorous
765 feeding. *Scientia Marina* **61**, 141-158.
766 Klinkhammer G., Elderfield H. and Hudson A. (1983) Rare earth elements in seawater
767 near hydrothermal vents. *Nature* **305**, 185-188.
768 Lerche D. and Nozaki Y. (1998) Rare earth elements of sinking particulate matter in the
769 Japan Trench. *Earth Planet. Sci. Lett.* **159**, 71-86.
770 Masuzawa T. and Koyama M. (1989) Settling particles with positive Ce anomalies from
771 the Japan Sea. *Geophys. Res. Lett.* **16**, 503-506.
772 Murphy K. and Dymond J. (1984) Rare earth element fluxes and geochemical budget in
773 the eastern equatorial Pacific. *Nature* **307**, 444-447.
774 Nakai S., Halliday A.N. and Rea D.K. (1993) Provenance of dust in the Pacific Ocean.
775 *Earth Planet. Sci. Lett.* **119**, 143-157.
776 Nelson D. M., Tréguer P., Brzezinski M. A., Leynaert A. and Quéguiner B. (1995)
777 Production and dissolution of biogenic silica in the ocean: Revised global estimates,
778 comparison with regional data and relationship to biogenic sedimentation. *Global*

779 *Biogeochem. Cycle* **9**, 359-372.
780 Nozaki Y., Alibo D.S., Amakawa H., Gamo T. and Hasumoto H. (1999) Dissolved rare
781 earth elements and hydrography in the Sulu Sea. *Geochim. Cosmochim. Acta.* **63**,
782 2171-2181.
783 Nozaki Y. and Alibo D.S. (2003) Importance of vertical geochemical processes in
784 controlling the oceanic profiles of dissolved rare earth elements in the northeastern
785 Indian Ocean. *Earth Planet. Sci. Lett*. **205**, 155-172.
786 Nozaki Y. (2001) *Encyclopedia of Ocean Sciences* Vol. 2, J. H. Steel *et al*. eds., pp.
787 840-845, Academic Press.
788 Ohta, A. and Kawabe, I. (2000) Rare earth element partitioning between Fe
789 oxyhydroxide precipitates and aqueous NaCl solutions doped with $NaHCO_3$:
790 determinations of rare earth element complexation constants with carbonate ions.
791 *Geochem. J.* **34**, 349-454.
792 Ohta, A. and Kawabe, I. (2001) REE(III) adsorption onto Mn dioxide (δ-MnO_2) and Fe
793 oxyhydroxide: Ce(III) oxidation by δ-MnO_2. *Geochim. Cosmochim. Acta.* **65**,
794 695-703.
795 Oka A., Hasumi H., Obata H., Gamo T. and Yamanaka Y. (2009) Study on vertical
796 profiles of rare earth elements by using an ocean general circulation model. *Global*
797 *Biogeochem. Cycles* **23**, GB4025, doi:10.1029/2008GB003353.
798 Onodera J. and Takahashi K. (2009) Long-term diatom fluxes in response to
799 oceanographic conditions at Stations AB and SA in the central subarctic Pacific and
800 Bering Sea, 1990-1998. *Deep-Sea Res*. **I56**, 189-211.
801 Otosaka S. and Noriki S. (2000) REEs and Ma/Al ratio of settling particles: horizontal
802 transport of particulate material in the northern Japan Trench. *Mar. Chem*. **72**,
803 329-342.
804 Palmer M.R. (1985) Rare earth elements in foraminifera tests. *Earth Planet. Sci. Lett*.
805 **73**, 285-298.
806 Piepgras D.J. and Jacobsen S.B. (1988) The isotopic composition of neodymium in the
807 North Pacific. *Geochim. Cosmochim. Acta*. **52**, 1371-1381.
808 Piepgras D.J. and Jacobsen S.B. (1992) The behavior of rare earth elements in seawater:
809 precise determination of variations in the North Pacific water column. *Geochim.*
810 *Cosmochim. Acta*. **56**, 1851-1862.

811 Raiswell R., Canfield D.E. and Berner, R.A. (1994) A comparison of iron extraction
812 methods for the determination of degree of pyritisation and the recognition of
813 iron-limited pyrite formation. *Chem. Geol.* **111**, 101-110.
814 Redfield A.C., Ketchum B.H. and Richards F.A. (1963) The influence of organisms on
815 the composition of seawater. In: *The Sea* (ed. M.N. Hill). Wiley Interscience, New
816 York, pp. 26-27.
817 Rimstidt, J. D., Balog, A. and Webb, J. (1998) Distribution of trace elements between
818 carbonate minerals and aqueous solutions. *Geochim. Cosmochim. Acta*. **62**,
819 1851-1863.
820 Rudnick R.L. and Gao S. (2003) Composition of the continental crust, *In The Crust (ed.*
821 *R. L. Rudnick) Vol. 3 Treatise on Geochemistry* (eds. H.D. Holland and K.K. Turekian).
822 Elsevier-Pergamon, Oxford, pp. 1-64.
823 Sambrotto R.N., Goering J.J. and McRoy C.P. (1984) Large yearly production of
824 phytoplankton in the western Bering Strait. *Science* **225**, 1147-1150.
825 Scherer, M. and Seitz, H. (1980) Rare-earth element distribution in Holocene and
826 Pleistocene coral and their redistribution during diagenesis. *Chem. Geol.* **28**, 279-289.
827 Schwertmann U. (1991) Solubility and dissolution of iron oxides. *Plant and Soil* **130,**
828 1-25.
829 Shabani M. B., Akagi T., Shimizu H. and Masuda A. (1990) Determination of trace
830 lanthanides and yttrium in seawater by inductively coupled plasma mass spectrometry
831 after preconcentration with solvent extraction and back extraction. *Anal. Chem*. **62**,
832 2709-2714.
833 Sholkovitz E.R., Landing W.M. and Lewis B.L. (1994) Ocean particle chemistry: The
834 fractionation of rare earth elements between suspended particles and seawater.
835 *Geochim. Cosmochim. Acta*. **58**, 1567-1579.
836 Sholkovitz, E. and Shen, G.T. (1995) The incorporation of rare earth elements in modern
837 coral. *Geochim. Cosmochim. Acta.* **59**, 2749-2756.
838 Stemmann L., Jackson G.A. and Ianson D. (2004) A vertical model of particle size
839 distributions and fluxes in the midwater column that includes biological and physical
840 processes−Part I: model formulation. *Deep-Sea Res*. **51**, 865-884.
841 Tachikawa K., Jeandel C. and Dupré B. (1997) Distribution of rare earth elements and
842 neodymium isotopes in settling particle material of the tropical Atlantic Ocean
843 (EUMELI site). *Deep-Sea Res*. **11**, 1769-1792.
844 Tachikawa K., Jeandel C. and Roy-Barman M. (1999) A new approach to the Nd

residence time in the ocean: the role of atmospheric inputs. *Earth Planet. Sci. Lett.* **170**, 433-446.

Takahashi T. (1975) Carbonate chemistry of sea water and the calcite compensation depth in the oceans. *Cushman Foundation for Foraminiferal Research, Spec. Publ*., **13**, 11-26.

Takahashi K., Fujitani N., Yanada M. and Maita Y. (2000) Long-term biogenic fluxes in the Bering Sea and the central subarctic Pacific Ocean, 1990-1995. *Deep-Sea Res.* **47**, 1723-1759.

Takahashi K., Fujitani N. and Yanada M. (2002) Long term monitoring of particle fluxes in the Bering Sea and the central subarctic Pacific Ocean, 1990-2000. *Progress in Oceanogr.* **55**, 95-112.

Tsunogai S., Kusakabe M., Izumi H., Koike I. and Hattori A. (1979) Hydrographic features of the deep water of the Bering Sea – the sea of silica. *Deep-Sea Res.* **26/6A**, 641-659.

Yang X., Liu Y., Li C., Song Y., Zhu H., and Jin X. (2007) Rare earth elements of aeolian deposits in Northern China and their implications for determining the provenance of dust storms in Beijing. *Geomorphology* **87**, 365-377.

Zhang J. and Nozaki Y. (1996) Rare earth elements and yttrium in seawater: ICP-MS determinations in the East Caroline, Coral Sea and South Fiji basins of the western South Pacific Ocean. *Geochim. Cosmochim. Acta*. **60**, 4631-4644.

Zhong, S. and Mucci, A. (1995) Partitioning of rare earth elements (REEs) between calcite and seawater solutions at 25°C and 1 atm, and high dissolved REE concentrations. *Geochim. Cosmochim. Acta.* **59**, 443-453.

Appendix

Dissolution kinetics: A model to explain variations in the REE patterns of settling particles

Dimensions of variables are expressed in parentheses using T for time, L for length, and M for mass. The dissolution process can be broken down into the following components:

1) aggregation rate as a function of particle density

2) settling speed as a function of aggregation

3) extent of dissolution as a function of settling speed and surface area of the aggregated particles

879 The first process, aggregation, A (L^{-3}), can be expressed very simply as a term
880 proportional to the square of the particle density, P (ML^{-3}) (Kiorboe, 1997), a measure
881 of productivity:
882 $$A \propto P^2 \quad . \qquad \text{(A1)}$$
883 The proportionality constant is actually dependent on the processes of aggregation
884 (Kiorboe, 1997; Alldredge and Gotschalk, 1988). Aggregation increases the size of
885 particles and reduces their surface area to mass ratio. For convenience, particles are
886 regarded as spheres. The radius r (L) and the surface area of the particles in a unit
887 volume of water, S (L^{-1}), are
888 $$r \propto A^{1/6} \qquad \text{(A2)}$$
889 $$S \propto A^{-1/6} \qquad \text{(A3)}$$
890 The second process, the settling velocity V (LT^{-1}) is not uniform, but has a distribution
891 based on the Stokes equation (Stemmann et al., 2004). For convenience, it is expressed
892 simply as
893 $$V \propto r^2 \qquad \text{(A4)}$$
894 From eq. (A2)
895 $$V \propto A^{1/3} \qquad \text{(A5)}$$
896 Equation (A5) is consistent with the observation that the settling velocity increases with
897 depth (Berelson, 2002).
898 The third process, the extent of dissolution, E (ML^{-3}), is proportional to both contact
899 time t (T) and surface area:
900 $$E = \varphi S t , \qquad \text{(A6)}$$
901 where φ ($ML^{-2}T^{-1}$) is a proportionality constant. Contact time is proportional to the
902 distance that particles travel, D (L), and the reciprocal of the settling velocity. Therefore,
903 $$E \propto \frac{S}{V} D \qquad \text{(A7)}$$
904 $$\propto A^{-1/2} D \qquad \text{(A8)} \quad \text{[from eqs. (A3) and (A4)]}$$
905 $$= \Phi \frac{D}{P} \qquad \text{(A9)} \quad \text{[from eq. (A1)]}$$
906 In the above equations, the proportionality constants are not unique but have a
907 distribution. They may also be a function of water temperature (Gnanadesikan, 1999).
908 For the sake of simplicity, a unique proportionality constant Φ (M^2L^{-7}) is applied in eq.
909 (A9). This equation indicates that the dissolution of particles is proportional to the
910 reciprocal of the particle density in the geographical area of interest. The time required

for particles to travel a given distance is given by the following equation

$$t = \frac{D}{V} \propto P^{-\frac{2}{3}} \qquad \text{(A10)} \qquad \text{[from eqs. (A1) and (A5)]}$$

Honjo and Manganini (1993) and Honjo et al. (1995, 1999) estimated the settling velocity of particles from the time lag of the mass flux peaks of settling particles observed at different depths in a water column. The estimated velocity was as great as 100 m/day—but, in reality, when the particle density is smaller, the settling velocity must be smaller because of the lower extent of aggregation.

Incidentally, the amount of an element that is absorbed onto the settling particles is itself proportional to the reciprocal of the settling velocity and to the surface area, and a qualitative relationship, similar to that of dissolution, is observed with the opposite sign of Φ in eq. (A9). Tachikawa et al. (1997) reported adsorption of REEs onto settling particles. If this is true, the same equation is valid. This equation links the primary product or particle density with dissolution or absorption.

The dissolution rate of element *i* from uniform particles is

$$\frac{dm_i}{dt} = k_i C_i S, \qquad \text{(A11)}$$

where m_i (ML^{-3}) is the amount of *i* dissolved from the particles, k_i ($ML^{-2}T^{-1}$) is the second-order rate constant of dissolution ($k_i < 0$) from a unit area of particles and C_i (dimensionless) is the concentration of *i* in the particles. Thus, the concentration of the element is expressed as

$$PC_i = P^o C_i^o + dm_i, \qquad \text{(A12)}$$

where C_i^o is the initial concentration of the elements. When the change is small, the equation can be approximated to

$$C_i \approx C_i^o \left(1 + \frac{k_i S t}{P}\right). \qquad \text{(A13)}$$

From eqs (A6) and (A9), kDP^{-1} is substituted for St to give

$$C_i \approx C_i^o \left(1 + \frac{k_i f D}{P^2}\right), \qquad \text{(A14)}$$

where f ($ML^{-5}T$) is Φ/φ, the conversion factor of the two constants. The ratio of element *i* to element *j* in the particles is approximately

$$\frac{C_i}{C_j} \approx \frac{C_i^o\left(1+\frac{k_i fD}{P^2}\right)}{C_j^o\left(1+\frac{k_j fD}{P^2}\right)}. \quad \text{(A15)}$$

Figure A1 shows the results of calculations using Eq. (A15) for a set of $k_i f$s. The difference in productivity affects the position in the P-C_j/C_i plane more strongly than does the depth difference. Even order of magnitude depth differences do not spoil the hyperbolic relationship. This simplification seems to be supported by the data of Lerche and Nozaki (1998) (Fig. 7 e, f, g and h). Although the sampling depths for their data vary from 1174 to 8688 m, their plots are distributed rather similarly, showing progressive dissolution.

Eq. (A15) can be further approximated to

$$\frac{C_i}{C_j} \approx \frac{C_i^o}{C_j^o}\left[1+\frac{(k_i-k_j)fD}{P^2}\right]. \quad \text{(A16)}$$

Eq. (A16) implies that the concentration of an element in particles changes hyperbolically with particle density. In fact, for settling particles at Station SA, Onodera et al. (2009) reported a similar hyperbolic relationship between *Neodenticule seminae* contributions to biogenic silica and radiolarian fluxes. *N. seminae* is a dissolution-resistant species and the hyperbolic relationship may be explained by the same dissolution dynamics.

It should be noted that the concentration of an element in the siliceous fraction is actually given by the concentration ratio of the element to opal or residue, which can be represented by Si.

$$\sum \mathrm{REE} \approx C_{\mathrm{REE}}^o\left[1+\frac{(k_{\mathrm{LREE,\,MREE}}-k_{\mathrm{Si}})fD}{P^2}\right] \quad \text{(A17)}$$

Similarly, the Ce anomaly, Eu anomaly, and HREE index are given by:

$$\text{Ce anomaly} \approx \text{Ce anomaly}^o\left[1+\frac{(k_{\mathrm{Ce}}-k_{\mathrm{LREE}})fD}{P^2}\right] \quad \text{(A18)}$$

$$\text{Eu anomaly} \approx \text{Eu anomaly}^o\left[1+\frac{(k_{\mathrm{Eu}}-k_{\mathrm{MREE}})fD}{P^2}\right] \quad \text{(A19)}$$

$$\text{HREE index} \approx \text{HREE index}^o\left[1+\frac{(k_{\mathrm{HREE}}-k_{\mathrm{LREE}})fD}{P^2}\right] \quad \text{(A20)}$$

For the sake of convenience, in the above equations, La and Pr are collectively designated LREE, and Sm and Gd are collectively designated middle REE (MREE).

The settling particles collected by traps are a spectrum of particles settling at

965 different velocities: rapidly-sinking (more aggregated, less dissolved) particles and
966 slowly-sinking (less aggregated, more dissolved) particles. The observed data deviate
967 from the ideal lines expressed by Eqs. (A17) to (A20) toward the inner region of the
968 hyperbolic curve, as mixing of different particles follows functions of the reciprocal of
969 *P*.
970
971

Figure captions

Figure 1. Map showing the two sampling stations: Station AB (53.5°N, 177°W) and Station SA (49°N, 174°W). Other sampling stations whose data are used as reference in this study are also shown: TSP 47 39-1 (47°00'N, 161°08.2'E) and TSP 24 271-1 (24°17.2'N, 150°28.2'E) from Piepgras and Jacobsen, 1992; LM-6/11 (34°10'N, 141°57'E) from Lerche and Nozaki (1998); and A&N (34°41'N, 139°54'E) from Alibo and Nozaki (1999).

Figure 2. Fraction separation and fractions analyzed for REEs. Note that siliceous fractions in this study correspond to the sum of the acid-soluble fraction and residue of Lerche and Nozaki (1998).

Figure 3. Shale-normalized patterns of the bulk settling particles collected at Stations AB (a) and SA (b).

Figure 4. Shale-normalized patterns of the siliceous fractions of settling particles collected at Stations AB (a) and SA (b).

Figure 5. Shale-normalized patterns of the averaged difference between the bulk and siliceous fractions (bulk – siliceous fraction). Note that the difference corresponds to the acetic acid-soluble fraction, which was not analyzed in this study. Some difference values are negative due to sample heterogeneity (see text). Only patterns of averaged differences are shown.

Figure 6. Correlations between some REE-pattern features for the bulk samples and the total mass of settling particles. Ce anomaly (a), Eu anomaly (b), HREE index (c) and ΣREE (d). See Table 1 for definitions.

Figure 7. Correlations of some REE-pattern features for the siliceous fractions with opal amount (a, b, c and d) and total mass (e, f, g and h) of settling particles. Ce anomaly (a and e), Eu anomaly (b and f), HREE index (c and g) and ΣREE (d and h). On e, f, g and h, the sum of the acid leach and residue reported by Lerche and Nozaki (1998) are also plotted. Their sampling site is located in the Japan Trench (LM-6/11, Fig. 1)

and the sampled depths vary from ~1200 to ~9000 m. They did not report component analyses of the particles and no combined plot can be created against opal amounts. See Table 1 for definitions.

Figure 8. Fitting of the mixing model to the observed bulk settling particle data. Fitting parameters are shown in brackets. a: (ΣREE of the presumed carbonate phase in ng/g, ΣREE of the bulk without the presumed carbonate phase). b: (ΣREE of the presumed carbonate phase in ng/g, ΣREE of the bulk without the presumed carbonate phase, Ce anomaly of the presumed carbonate phase, Ce anomaly of the bulk without the presumed carbonate phase).

Figure 9. Distribution ratios of REEs between acetic acid-soluble fraction and seawater reported for (a) settling particles and (b) suspended particles collected on filters. Averages are shown in open circles.
Settling particles were collected from four different depths (1174, 3680, 5687, and 8688 m). Seawater data are for samples collected from depths close to the sediment trap (994, 3997, 5957, and 8654 m) (Lerche and Nozaki, 1998). Averages are for all data shown in the figure. Vertical axis: (μg/g settling particles)/(ng/kg seawater)
Seawater samples with suspended particles were collected from 10 different depths from surface to 2000 m (Sholkovitz et al., 1994). Averages are from the five data sets deeper than 300 m. Note that the distribution factors are almost constant. Vertical axis: (mol/kg seawater)/(mol/kg seawater)

Figure 10. Fitting of the plots with the working equations of dissolution dynamics. Ce anomaly (a), Eu anomaly (b), HREE index (c) and ΣREE (d). The data obtained by Lerche and Nozaki (1998) are shown as crosses. The amount of opal is estimated as 20±10% of the total mass. Three data for the samples from depth 3680 m, which is closest to our sampled depths, are selected. See Table 1 for definitions.

Figure 11. Examples of vertical profiles of dissolved REEs reported for the North Pacific Ocean. The profiles are normalized to range from 0 to 1.
a and b: Piepgras and Jacobsen (1992); c: Alibo and Nozaki (1999). The vertical profile of dissolved silica (Piepgras and Jacobsen, 1988) is also shown. See Fig. 1 for the locations of the sampling stations.

Figure 12. Schematic diagram showing the behavior of different components of settling particles and REE fractionation/distribution processes inferred by this study.

Figure A1. Simulation of the relationship between opal amount and fractionation of elements at several depths. The set of dissolution rates used is (kk_{Si}, kk_i, kk_j) = (0.1, 0.006, 0.01), where *Si*, *i*, and *j* represent opal, LREEs, and HREEs, respectively. Depth scale = 0.5 corresponds to the distance at which 0.5‰ of Si dissolves from the original particles when opal flux is 1000 $mgm^{-2}d^{-1}$. The depth scale is linear with distance. Note that depth differences of even several factors do not spoil the hyperbolic relationship seen in Fig. 10.

Tables and Figures

Table 1. REE concentration (ng/g) of bulk settling particles collected monthly using the sediment trap set at the North Pacific Ocean along with the some features of shale-normalized REE patterns and component data[a].

Site	AB													SA											
No.	6#1	6#2	6#3	6#4	6#5	6#6	6#7	6#8	6#9	6#10	6#11	6#12	6#13	7#1	7#2	7#3	7#4	7#5	7#6	7#7	7#8	7#9	7#10	7#11	7#12	7#13
Mid Date	15 Aug.	2 Sep.	22 Sep.	12 Oct.	9 Nov.	25 Dec.	19 Feb.	29 Mar.	18 Apr.	8 May	28 May	17 Jun.	13 Jul.	26 Aug.	22 Sep.	12 Oct.	3 Nov.	19 Dec.	19 Feb.	29 Mar.	18 Apr.	8 May	28 May	17 Jun.	7 Jul.	25 Jul.
La	1280	1100	1630	1670	1480	1750	4070	3230	1010	761	1320	562	1120	3510	3060	3450	4350	4830	4220	4360	3420	3410	4590	2060	2300	2280
Ce	2420	2040	3220	2740	2100	2810	7160	5870	1870	1440	2620	1060	1800	5780	5220	4220	5250	6170	6340	6680	4910	4920	7190	2560	3060	3100
Pr	358	292	456	436	382	464	1120	863	300	206	356	150	265	923	816	913	1180	1340	1180	1210	938	909	1280	570	647	632
Nd	1380	1100	1730	1560	1430	1810	4380	3210	1060	793	1390	583	989	3560	2940	3200	4410	5080	4440	4490	3440	3270	4920	2300	2420	2220
Sm	327	272	428	366	339	419	1050	773	249	178	314	128	238	813	675	727	1020	1190	1030	1070	738	751	1170	548	574	516
Eu	54.3	36.5	92.7	93.1	60.5	77.1	190	189	59.3	39.4	72.2	32.8	40.6	116	127	129	146	177	135	221	200	198	283	136	138	95.3
Gd	351	295	466	399	371	463	1170	837	267	192	338	135	246	805	718	725	1040	1170	1040	1120	843	782	1200	519	614	502
Tb	54.0	44.7	68.5	60.7	55.1	66.6	173	119	38.5	27.4	46.8	19.9	37.3	125	106	119	154	175	152	168	128	112	177	75.9	90.7	78.2
Dy	340	267	403	378	329	406	1050	687	242	180	283	127	228	742	637	694	891	996	871	935	713	655	1070	471	542	453
Ho	72.0	56.9	86.0	90.4	68.7	94.2	219	146	52.6	39.9	65.1	31.0	53.7	154	129	142	183	195	171	193	154	135	227	105	113	114
Er	236	187	271	260	218	260	695	466	182	126	200	89.9	160	485	403	446	554	583	525	591	435	392	622	312	363	310
Tm	35.2	27.6	41.8	38.7	32.3	38.1	98.2	66.5	22.5	16.7	26.2	12.4	21.5	69.2	55.6	61.2	78.4	82.9	73.3	79.4	56.9	58.3	86.0	45.8	51.0	41.0
Yb	239	200	294	271	219	256	666	448	161	127	185	85.6	157	469	395	458	505	532	471	554	385	366	564	329	360	268
Lu	51.5	58.0	67.1	52.2	42.0	53.1	145	88.7	28.0	20.6	29.9	13.5	28.3	87.5	74.0	81.7	94.9	101	92.1	92.5	75.9	77.5	101	63.3	66.5	61.0
Ce anomaly	0.82	0.83	0.86	0.74	0.65	0.72	0.77	0.81	0.78	0.84	0.88	0.85	0.76	0.74	0.76	0.55	0.53	0.56	0.66	0.67	0.63	0.65	0.68	0.54	0.58	0.60
Eu anomaly	0.75	0.61	0.98	1.15	0.80	0.82	0.81	1.10	1.08	1.01	1.04	1.18	0.79	0.67	0.86	0.83	0.66	0.70	0.61	0.95	1.19	1.22	1.13	1.20	1.09	0.88
HREEindex	2.79	2.95	2.68	2.30	2.13	2.17	2.48	2.05	2.28	2.24	1.94	2.10	1.96	1.93	1.84	1.82	1.73	1.64	1.68	1.78	1.69	1.65	1.79	2.25	2.22	1.87
ΣREE/1000	7.19	5.97	9.26	8.42	7.14	8.97	22.2	17.0	5.53	4.15	7.25	3.03	5.39	17.6	15.3	15.4	19.9	22.6	20.7	21.8	16.4	16.0	23.5	10.1	11.3	10.7
Flux data of component (mg m^{-2} d^{-1})																										
Total mass	349.2	135.3	116.8	152.5	172.2	103.9	80.3	170.9	895.2	1221.6	584.1	395.5	378.1	173.2	95.9	141.7	121.2	42.5	40.2	61.3	57.4	113.1	78.7	233.4	133.8	64.0
Opal	221.7	89.5	79.0	97.0	95.3	61.3	48.4	106.8	605.2	805.0	372.7	260.7	224.2	100.1	49.6	61.6	57.2	22.9	22.8	33.5	29.9	54.4	39.4	141.9	73.5	36.2
$CaCO_3$	12.2	11.7	24.2	30.1	54.1	19.5	12.6	26.3	46.3	60.1	33.1	20.4	23.6	31.0	18.9	58.7	45.8	13.6	9.1	15.5	17.9	51.4	26.6	51.1	31.8	17.8
Org. C	10.8	4.1	3.8	5.4	5.5	3.7	3.2	5.7	21.2	29.6	10.3	8.7	9.7	6.4	3.7	5.4	3.7	1.2	1.2	1.9	1.7	2.4	1.9	10.2	5.1	1.8
Residue	91.6	25.2	5.3	13.5	10.8	15.0	12.1	25.1	197.1	291.4	155.6	95.4	109.0	30.5	20.7	11.7	11.5	3.8	6.2	8.7	6.4	3.0	9.3	22.0	19.4	6.8

The definitions of the features of a REE pattern are

$$\text{Ce anomaly} = \frac{(\text{Ce})_n}{\sqrt{(\text{La})_n (\text{Pr})_n}} \qquad \text{Eu anomaly} = \frac{(\text{Eu})_n}{\sqrt{(\text{Sm})_n (\text{Gd})_n}} \qquad \sum \text{REE} = \sum [\text{Ln}] \qquad \text{HREE index} = \frac{(\text{Er})_n + (\text{Tm})_n + (\text{Yb})_n + (\text{Lu})_n}{4(\text{La})_n}$$

where, Ln is an REE element, and [Ln] and $(Ln)_n$ denote the concentration and shale normalized value of Ln, respectively.

a) Component data from Ashahi and Takahashi (2007). Note that the data of residue may be associated with considerable errors, as errors of all other components accumulate.

Table 2 REE concentration (ng/g) of the siliceous fraction of the settling particles[a)] collected using the sediment trap set at the North Pacific Ocean along with some features of the REE patterns.

Site	AB													SA											
No.	6#1	6#2	6#3	6#4	6#5	6#6	6#7	6#8	6#9	6#10	6#11	6#12	6#13	7#1	7#2	7#3	7#4	7#5	7#6	7#7	7#8	7#9	7#10	7#11	7#12	7#13
Mid Date	15 Aug.	2 Sep.	22 Sep.	12 Oct.	9 Nov.	25 Dec.	19 Feb.	29 Mar.	18 Apr.	8 May	28 May	17 Jun.	13 Jul.	26 Aug.	22 Sep.	12 Oct.	3 Nov.	19 Dec.	19 Feb.	29 Mar.	18 Apr.	8 May	28 May	17 Jun.	7 Jul.	25 Jul.
La	912	778	1020	1550	1190	1840	2210	988	1210	736	1130	1190	1130	3250	3120	2980	2830	3040	3040	1230	1100	848	-	761	-	1560
Ce	2030	1800	2390	2920	2780	4770	5500	2250	2700	1720	2590	4390	2650	7200	7290	6380	6440	7580	7910	2750	2480	2410	-	1760	-	4100
Pr	245	186	254	327	335	497	595	266	336	193	314	263	296	870	850	743	757	806	783	294	261	190	-	181	-	401
Nd	956	685	975	1270	1250	1960	2210	997	1290	730	1170	992	1060	3250	3030	3090	2830	3090	2940	1030	909	668	-	638	-	1450
Sm	239	148	224	296	285	475	488	225	283	158	258	207	226	753	647	608	617	664	647	207	200	132	-	122	-	297
Eu	50.5	36.2	45.0	67.3	60.7	121	102	61.1	70.2	40.2	65.1	57.9	59.9	158	135	119	141	136	141	51.1	44.7	32.0	-	30.8	-	62.9
Gd	231	164	225	326	320	488	519	243	291	160	271	235	245	721	655	584	596	675	645	221	190	144	-	122	-	320
Tb	32.9	22.2	31.9	44.3	42.6	63.6	66.1	38.4	49.7	25.0	42.6	34.0	37.3	105	94.0	79.6	84.2	89.3	83.0	34.1	28.7	21.3	-	19.5	-	42.2
Dy	205	144	213	283	266	386	403	236	314	161	273	205	238	638	581	503	543	555	545	223	194	142	-	129.2	-	268.7
Ho	43.6	30.3	47.1	62.5	58.0	88.1	94.5	50.9	68.0	35.3	58.0	44.0	50.6	142	121	111	119	120	121	44.8	47.1	31.5	-	29.0	-	61.0
Er	136	96.7	147	186	179	255	277	171	223	114	192	145	164	406	369	330	334	371	348	159	141	92.0	-	92.3	-	170
Tm	23.0	17.8	22.0	31.6	28.5	41.6	40.8	25.3	31.6	16.4	27.2	20.7	25.1	61.0	57.4	46.8	54.2	57.2	57.5	24.6	23.0	13.2	-	14.4	-	25.3
Yb	157	125	157	215	196	275	283	171	229	118	196	146	183	427	391	339	353	378	424	163	156	92.6	-	104	-	194
Lu	28.6	27.7	34.5	39.9	37.5	50.5	51.8	28.2	37.7	18.5	31.1	25.1	29.6	74.9	83.4	67.6	61.5	66.0	82.5	25.2	25.3	15.8	-	17.0	-	38.8
Ce anomaly	0.99	1.09	1.08	0.95	1.01	1.15	1.11	1.01	0.98	1.05	1.00	1.81	1.06	0.99	1.03	0.98	1.01	1.12	1.18	1.05	1.07	1.38		1.10		1.20
Eu anomaly	1.01	1.09	0.94	1.02	0.95	1.18	0.96	1.23	1.15	1.19	1.16	1.24	1.20	1.01	0.98	0.94	1.10	0.95	1.03	1.12	1.08	1.09		1.19		0.96
HREEindex	2.37	2.28	2.25	1.92	2.31	2.11	1.81	2.40	2.57	2.14	2.33	1.70	2.14	1.81	1.84	1.63	1.75	1.75	1.90	1.80	1.92	1.51		1.81		1.72
ΣREE/1000	5.29	4.26	5.79	7.61	7.03	11.3	12.8	5.75	7.13	4.23	6.62	7.95	6.39	18.1	17.4	15.9	15.8	17.6	17.8	6.46	5.79	4.83		4.03		8.98

a) Note that two different aliquots of sample suspension were used for the analyses of bulk and siliceous fractions.

- not measured. See Table 1 for the definitions of Ce anomaly, Eu anomaly, HREE index and ΣREE.

Table 3 Results of sequential leaching in μg/g (percent distribution)

Sample	reagent	Mn	Fe	Al	Si/Al[b]
AB6#5	Acetic acid	81 (60)	290 (11)	400 (9)	
(172.2)[a]	HCl	17 (12)	280 (11)	250 (6)	60.0 [64.8]
	HF	37 (28)	1990 (78)	3600 (85)	
AB6#9	Acetic acid	22 (34)	80 (3)	150 (3)	
(895.2)[a]	HCl	5 (9)	160 (7)	200 (4)	65.6 [81.0]
	HF	37 (57)	2180 (90)	4100 (92)	
SA7#4	Acetic acid	121 (68)	400 (8)	600 (8)	
(121.2)[a]	HCl	7 (4)	510 (11)	300 (4)	27.4 [31.3]
	HF	50 (28)	3870 (81)	6900 (88)	
SA7#8	Acetic acid	171 (73)	430 (14)	1050 (17)	
(57.36)[a]	HCl	28 (12)	410 (11)	200 (3)	45.4 [52.4]
	HF	36 (15)	2770 (75)	4600 (79)	

a) Total mass (mg m^{-2} day^{-1})

b) Si concentration in opal [in opal + residue] is divided by the concentration of Al in HCl+HF leached fractions. Opal (SiO_2+0.4H_2O) values in Table 1 are multiplied with 0.477 to obtain Si. 30% of residue is assumed to be composed of Si.

c) Detection limits of Mn, Fe, and Al are 1, 10, and 50 μg/g, respectively.

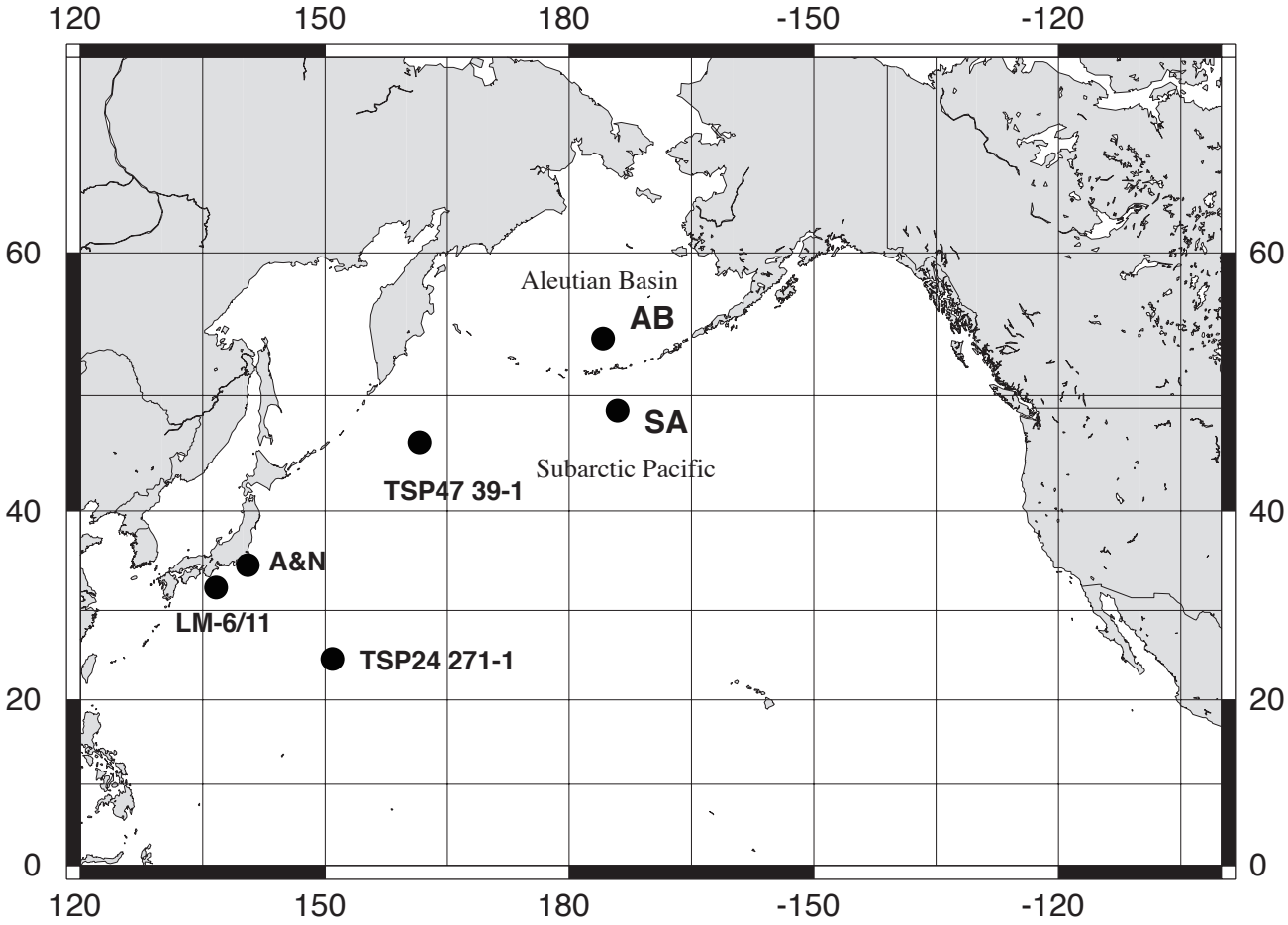

Fig. 1 Akagi et al.

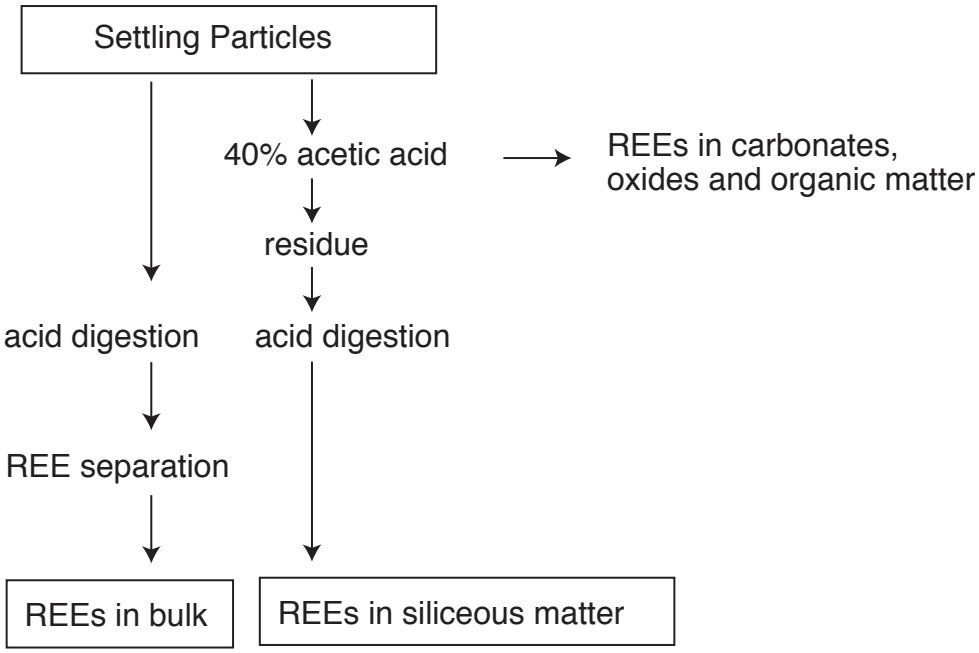

Fig. 2 Akagi et al.

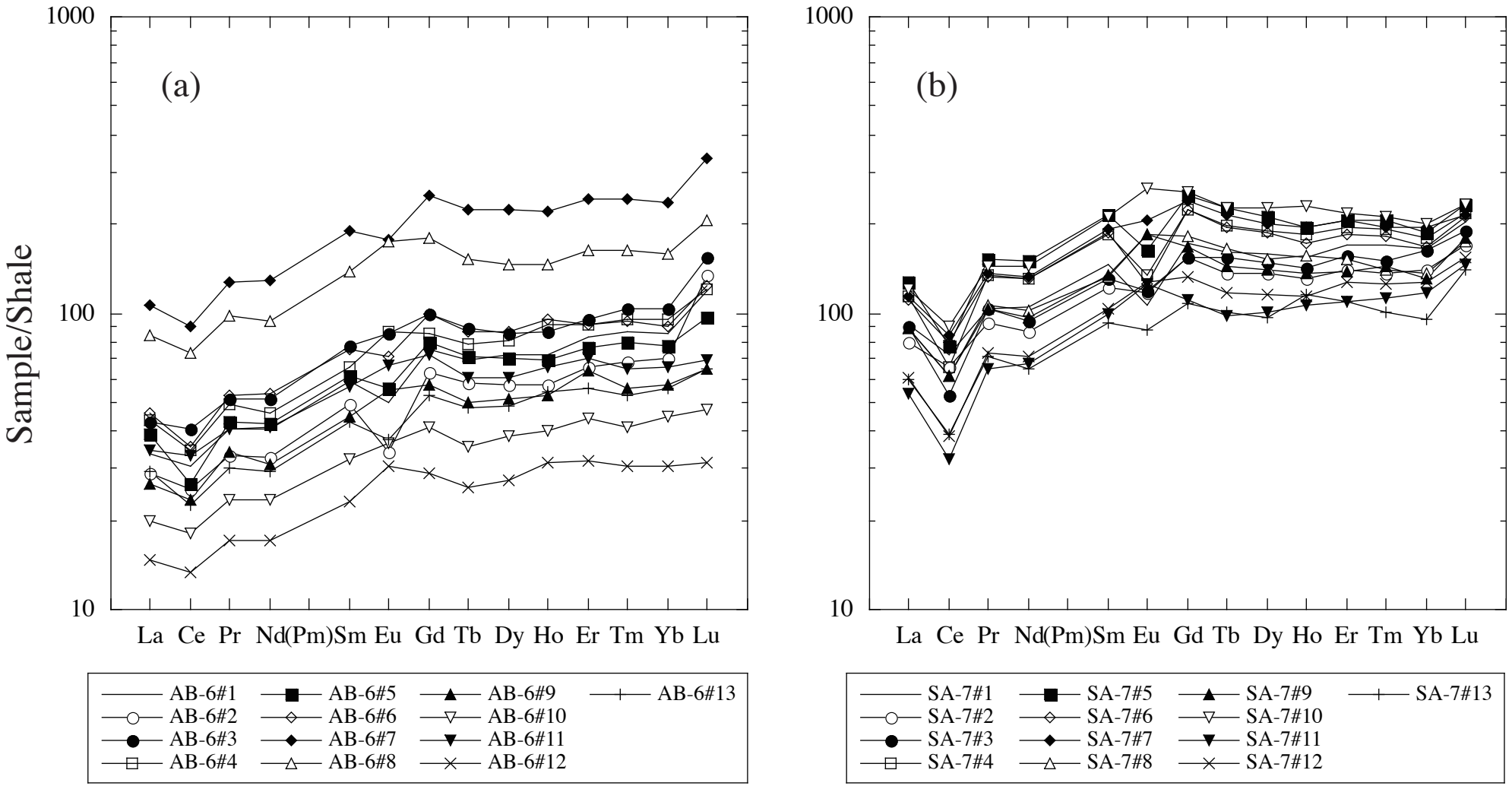

Fig. 3 Akagi et al.

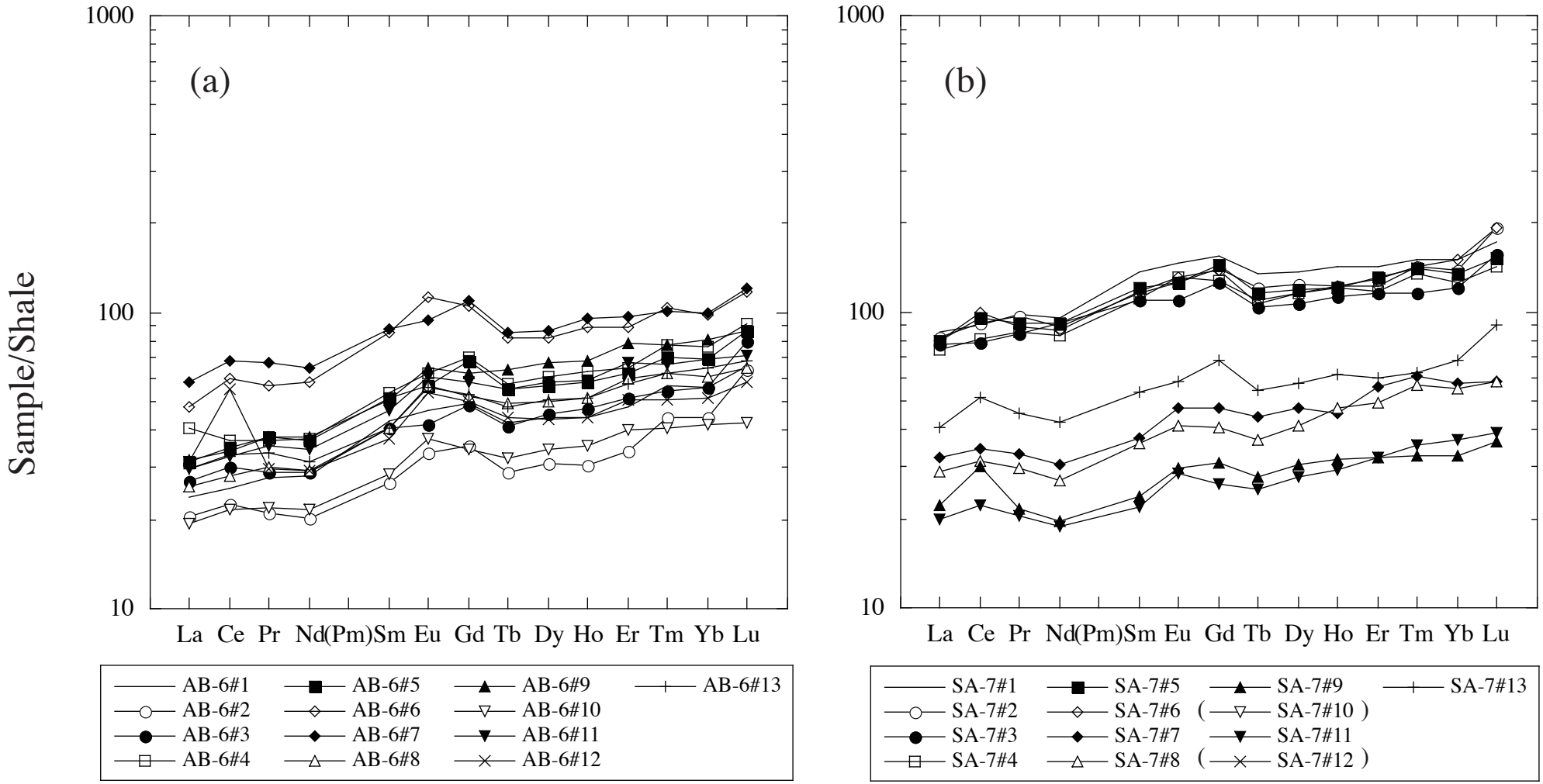

Fig. 4 Akagi et al.

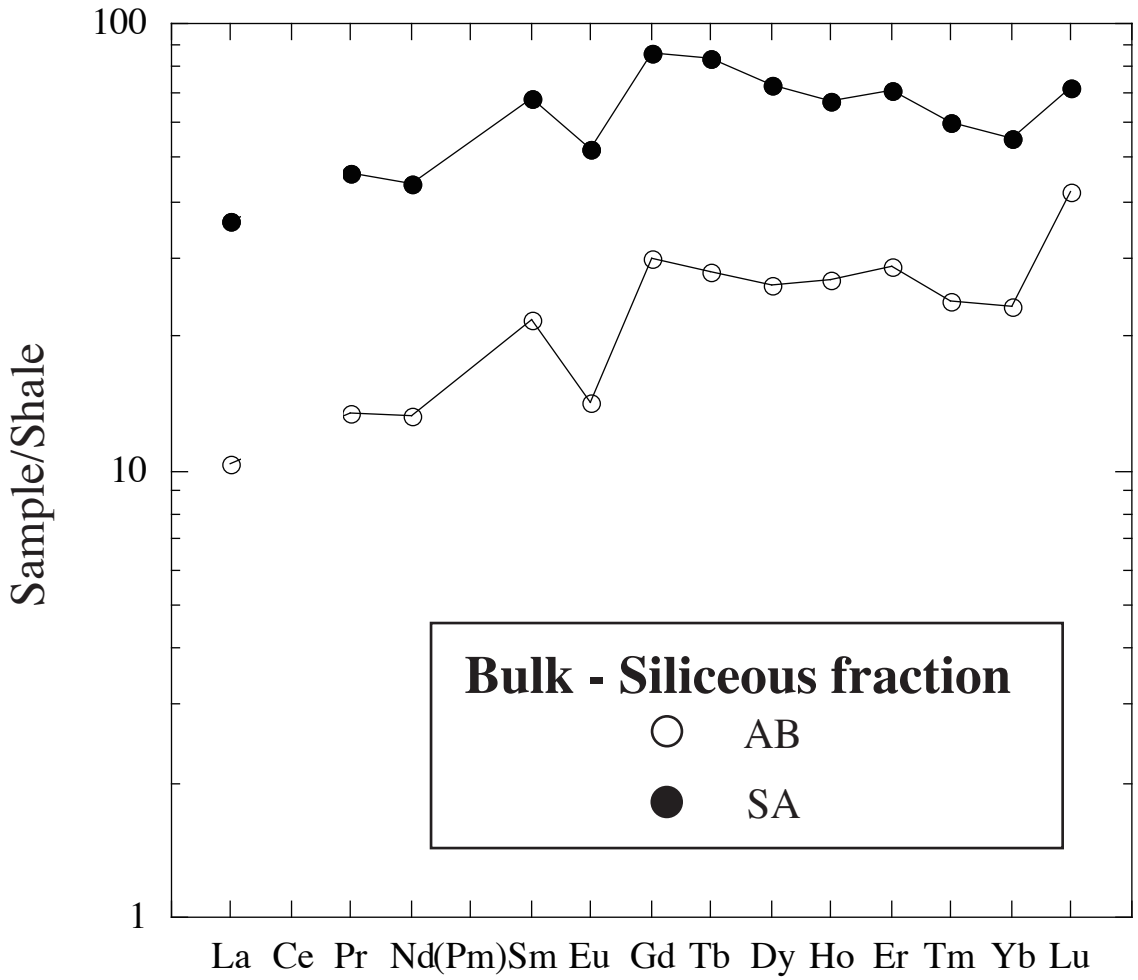

Fig. 5 Akagi et al.

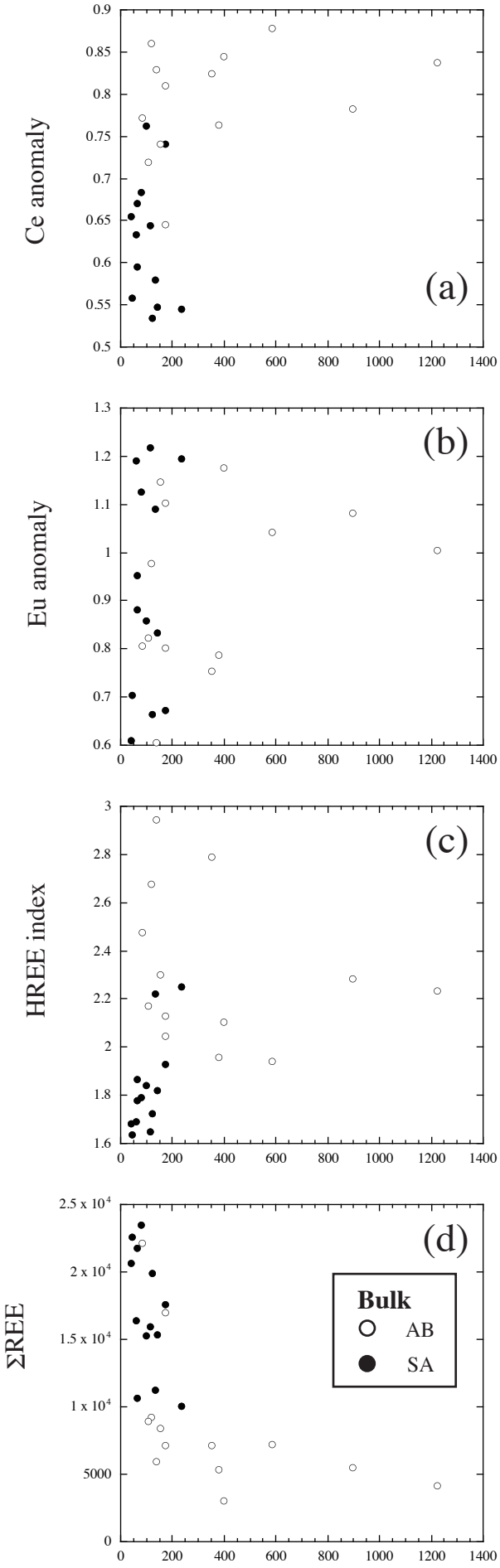

Fig. 6 Akagi et al.

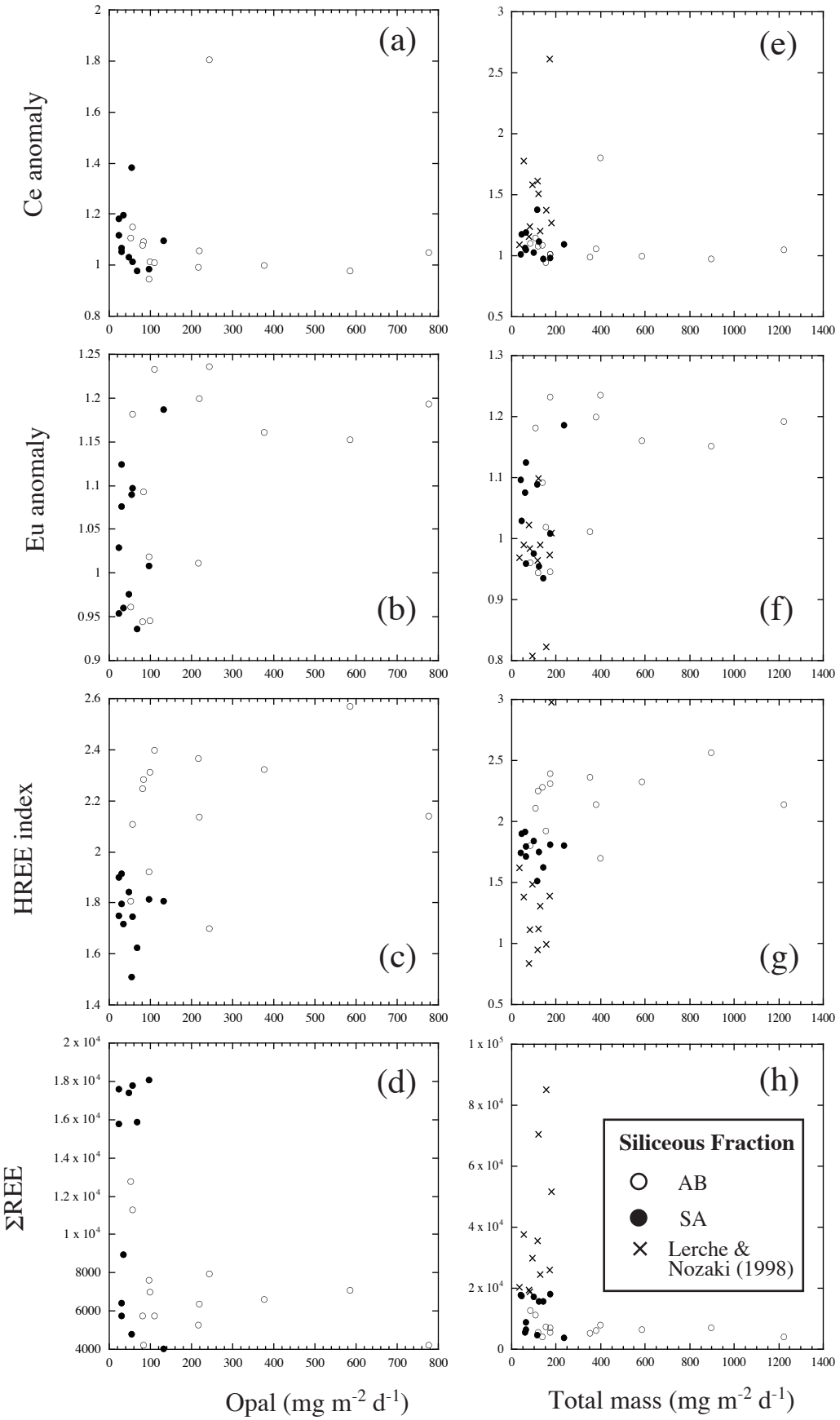

Fig. 7 Akagi et al.

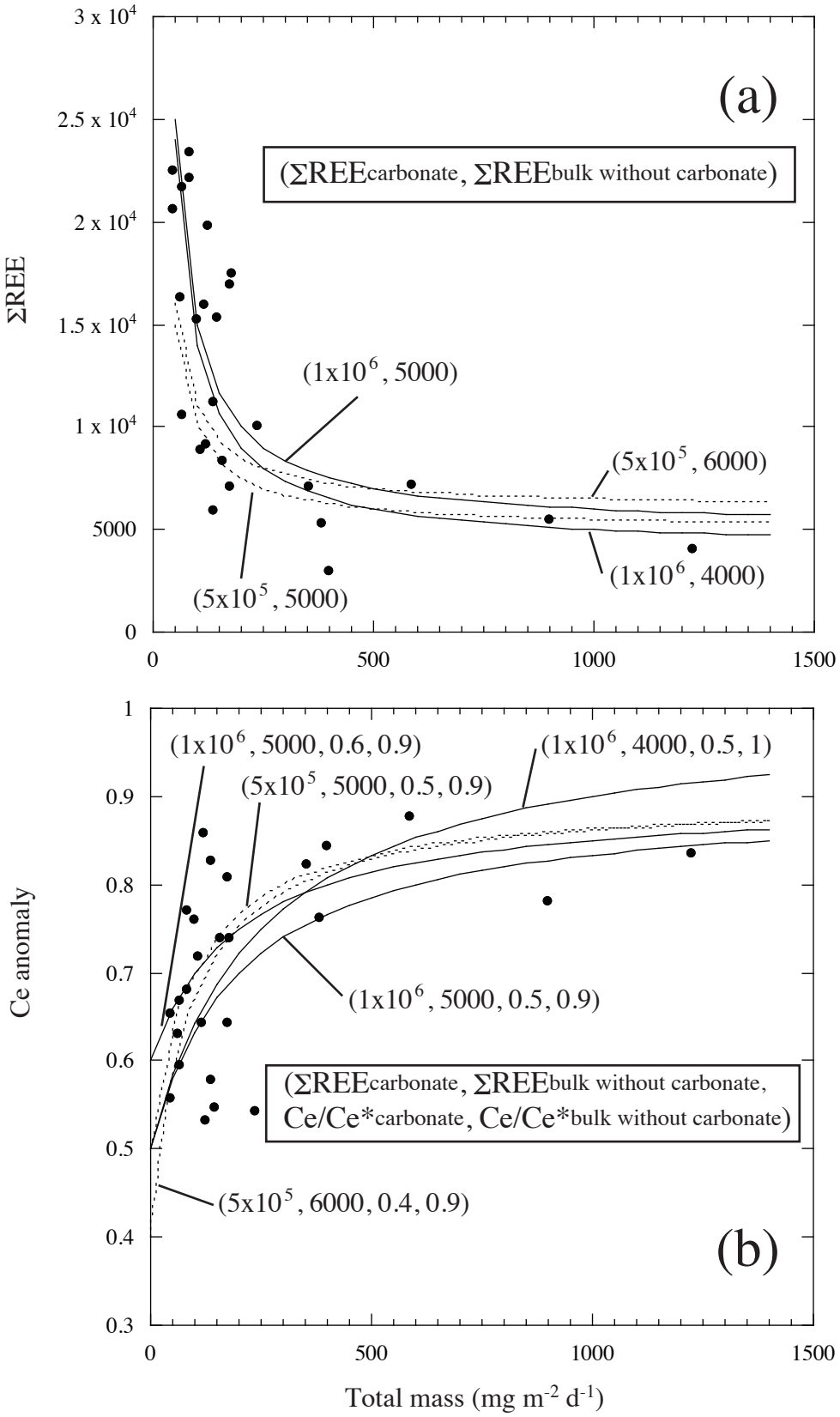

Fig. 8 Akagi et al.

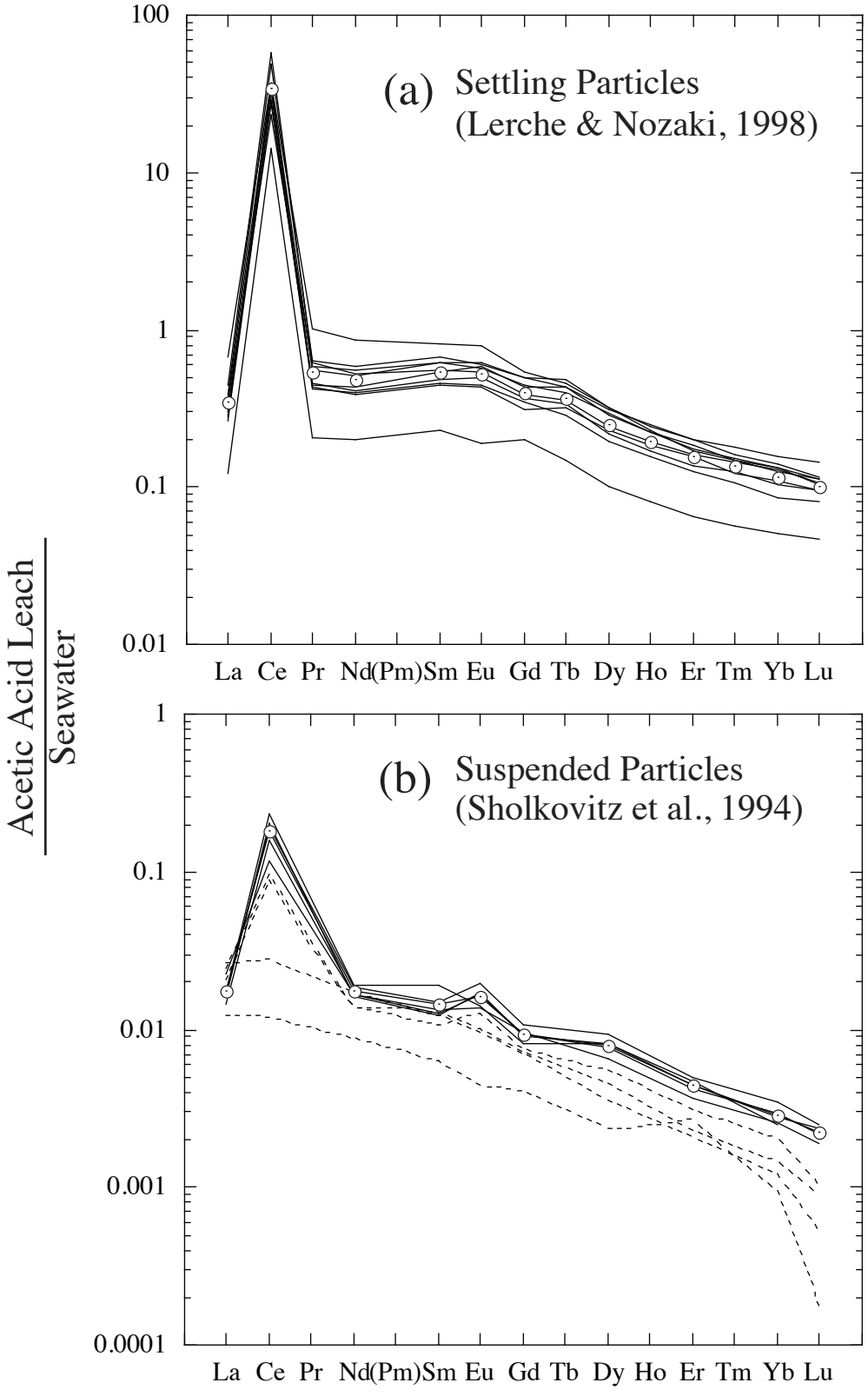

Fig. 9 Akagi et al.

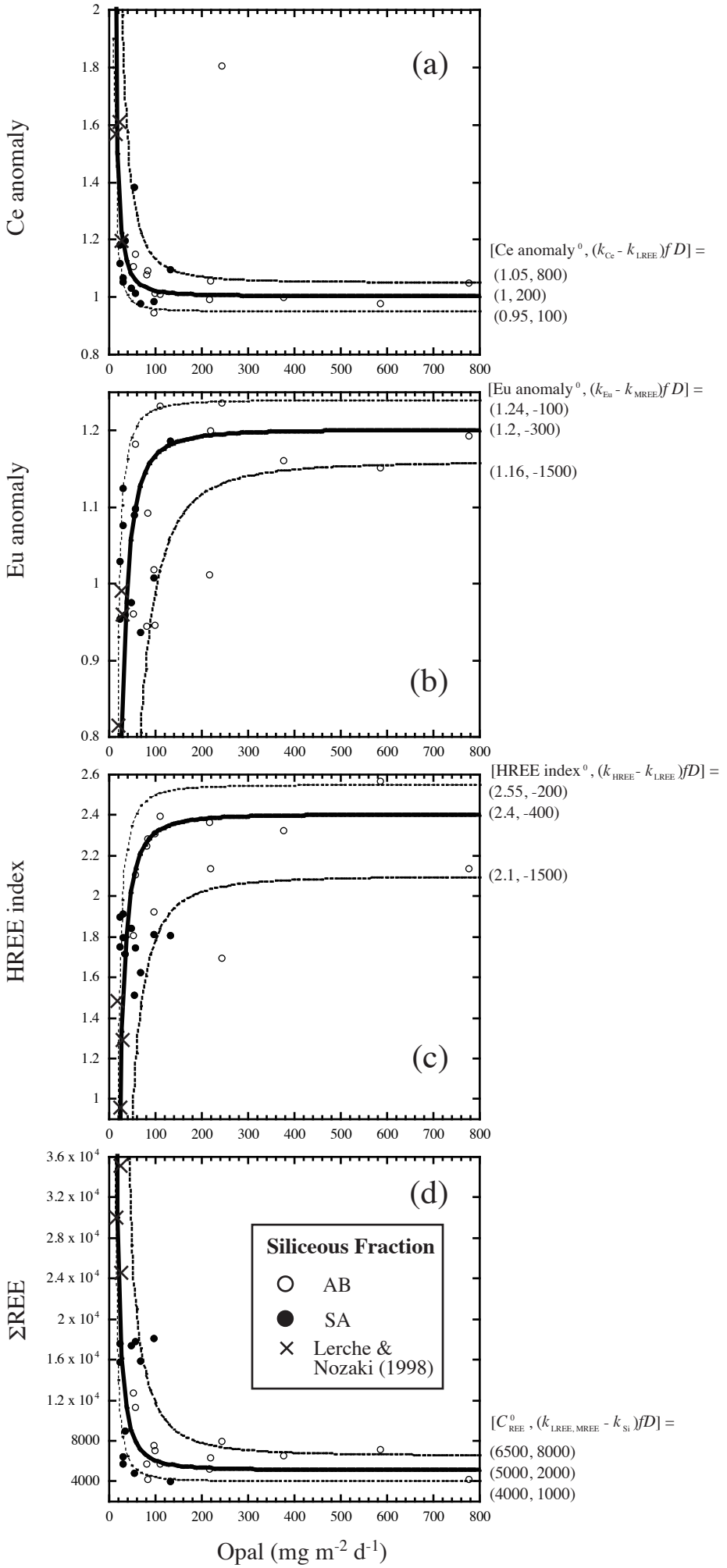

Fig. 10 Akagi et al.

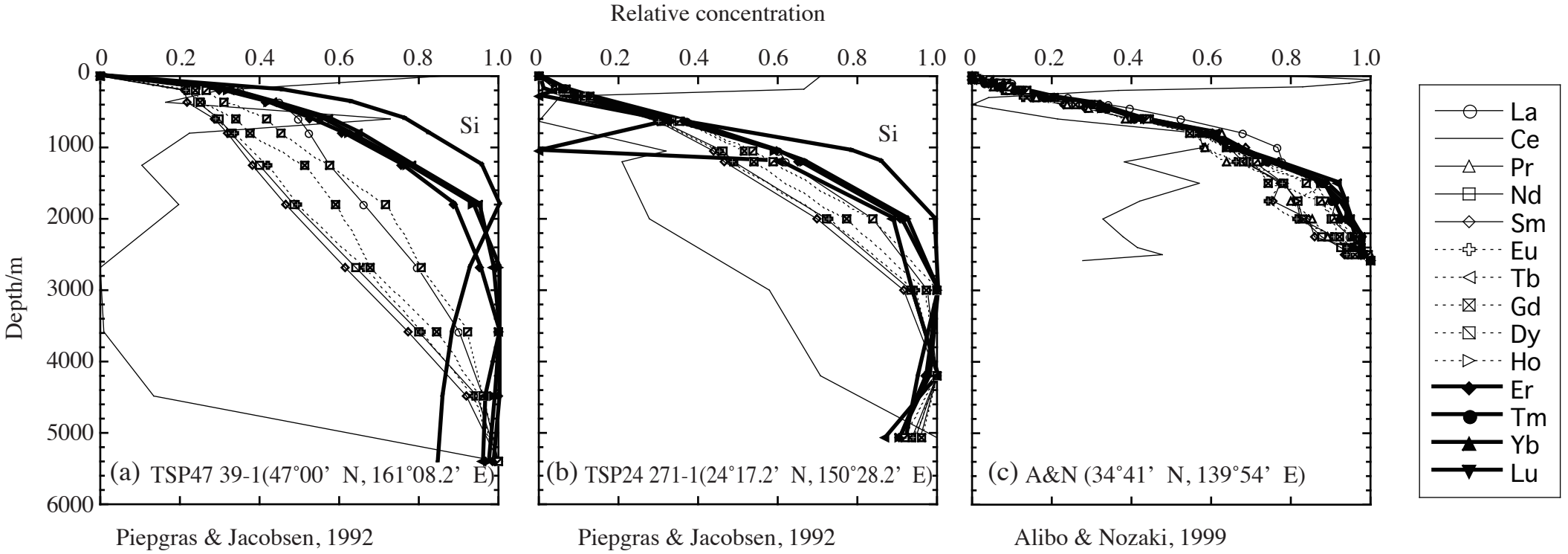

Figure 11. Akagi et al.

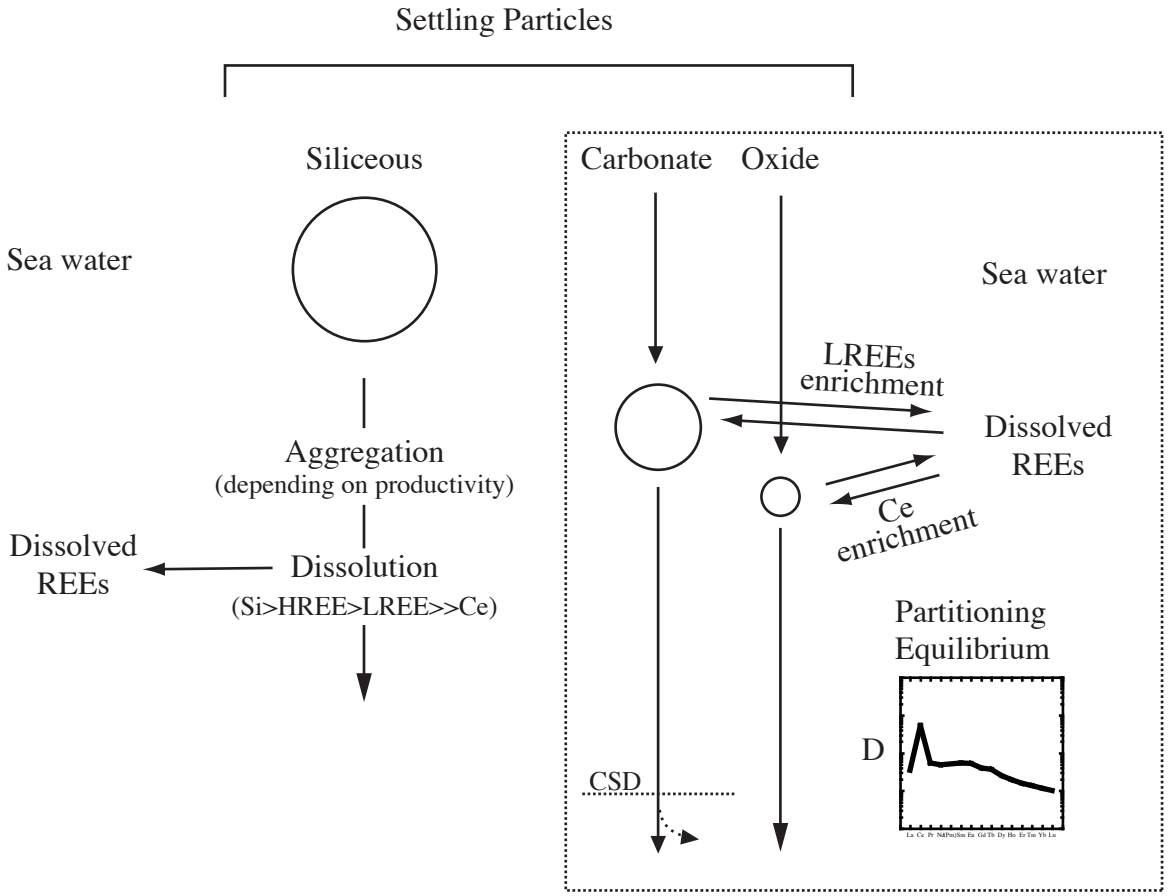

Fig. 12 Akagi et al.

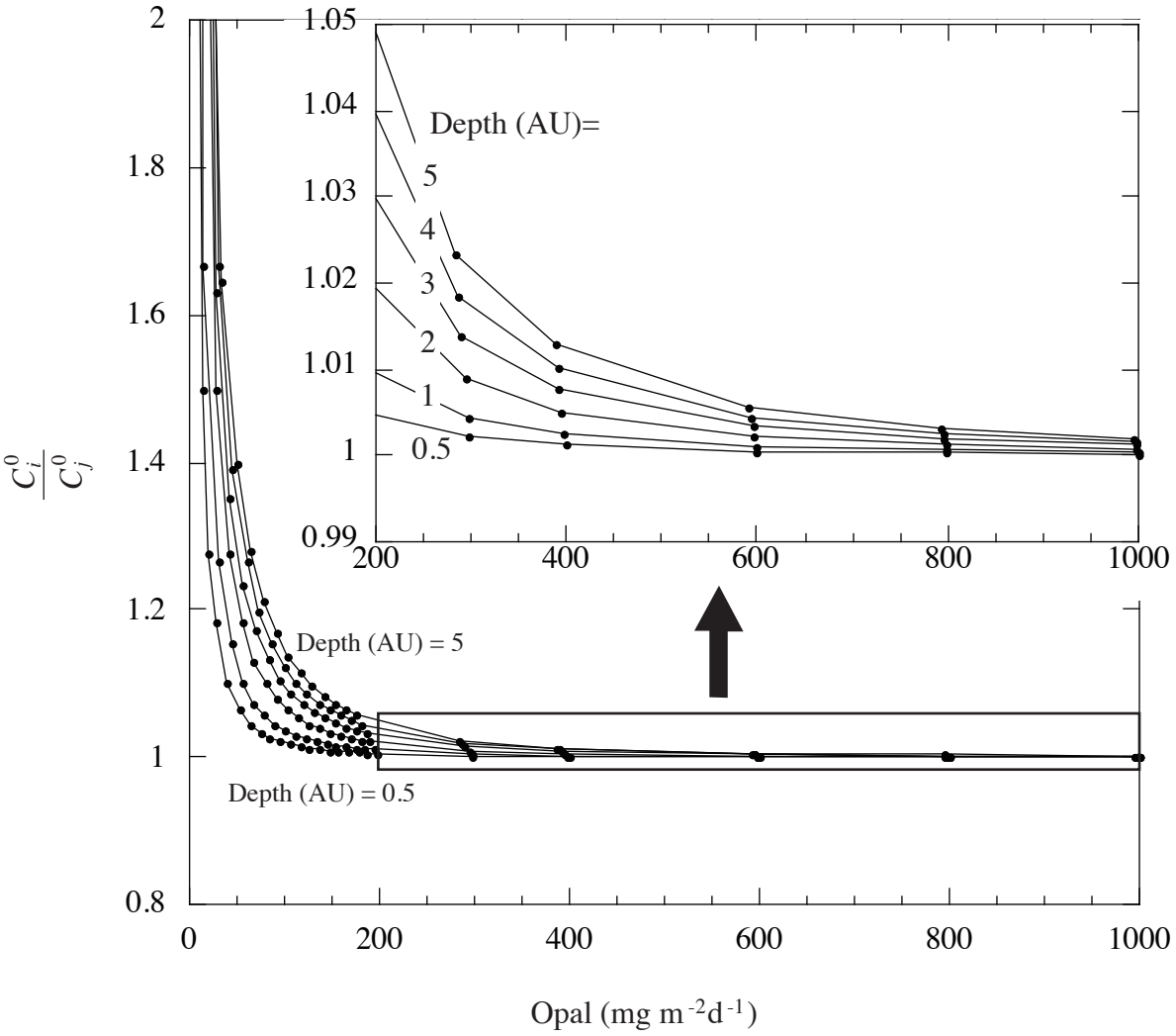

Fig. A1 Akagi et al.